

The SCUBA Local Universe Galaxy Survey I. First Measurements of the Submillimetre Luminosity and Dust Mass Functions

Loretta Dunne¹, Stephen Eales¹, Michael Edmunds¹, Rob Ivison²,
Paul Alexander³ and David L. Clements¹

¹*Department of Physics and Astronomy, University of Wales Cardiff, PO Box 913, Cardiff, CF2 3YB*

²*Department of Physics and Astronomy, University College London, Gower Street, London WC1E 6BT*

³*Department of Astrophysics, Cavendish Laboratory, Madingley Road, Cambridge CB3 0HE*

22 March 2021

ABSTRACT

This is the first of a series of papers presenting results from the SCUBA Local Universe Galaxy Survey (SLUGS), the first statistical survey of the submillimetre properties of the local universe. As the initial part of this survey, we have used the SCUBA camera on the James Clerk Maxwell Telescope to observe 104 galaxies from the IRAS Bright Galaxy Sample. We present here the 850 μ m flux measurements.

The 60, 100, and 850 μ m flux densities are well fitted by single-temperature dust spectral energy distributions, with the sample mean and standard deviation for the best-fitting temperature being $T_d = 35.6 \pm 4.9$ K and, for the dust emissivity index $\beta = 1.3 \pm 0.2$. The dust temperature was found to correlate with 60 μ m luminosity. The low value of β may simply mean that these galaxies contain a significant amount of dust that is colder than these temperatures. We have estimated dust masses from the 850 μ m fluxes and from the fitted temperature, although if a colder component at around 20 K is present (assuming a β of 2) then the estimated dust masses are a factor of 1.5–3 too low.

We have made the first direct measurements of the submillimetre luminosity function (LF) and of the dust mass function. Unlike the *IRAS* 60 μ m LF, these are well fitted by Schechter functions. The slope of the 850 μ m LF at low luminosities is steeper than -2 , implying that the LF must flatten at luminosities lower than we probe here. We show that extrapolating the 60 μ m LF to 850 μ m using a single temperature and β does not reproduce the measured submillimetre LF. A population of ‘cold’ galaxies ($T_d < 25$ K) emitting strongly at submillimetre wavelengths would have been excluded from the 60 μ m selected sample. *IF* such galaxies do exist then this estimate of the 850 μ m is biased (it is underestimated). Whether such a population does exist is unknown at present.

We have correlated many of the global galaxy properties with the FIR/submillimetre properties. We find that there is a tendency for less luminous galaxies to contain hotter dust and to have a greater star-formation efficiency (cf. Young 1999). The average gas-to-dust ratio for the sample is 581 ± 43 (using both the atomic and molecular hydrogen) which is significantly higher than the Galactic value of 160. We believe this discrepancy is likely to be due to a ‘cold dust’ component at $T_d \leq 20$ K. There is a surprisingly tight correlation between dust mass and the mass of molecular hydrogen, estimated from CO measurements, with an intrinsic scatter of $\simeq 50$ per cent.

Key words: dust, extinction; galaxies – ISM – galaxies; luminosity function, mass function – galaxies; starburst – infrared; galaxies – submillimetre.

1 INTRODUCTION

With the advent of the SCUBA bolometer array (Holland et al. 1999) on the James Clerk Maxwell Telescope* it has, for the first time, become feasible to map the submillimetre ($100\mu\text{m} < \lambda < 1\text{ mm}$) emission of a large (>100) sample of galaxies. While this may seem a paltry feat in comparison to surveys conducted at other wavelengths, submillimetre astronomy has lagged behind the rest due to the technical difficulties of building sensitive enough instruments. Until recently, all that existed were a handful of submillimetre fluxes of nearby galaxies made with single element bolometers (Eales, Wynn-Williams & Duncan 1989; Stark et al. 1989; Clements, Andreani & Chase 1993). No information about the distribution of the dust was available and even the fluxes themselves were subject to considerable uncertainty, especially when beam corrections had to be made in order to compare with measurements in the far infra-red (FIR : $10\mu\text{m} < \lambda < 100\mu\text{m}$) made with the *IRAS* satellite. Quite surprisingly, even before SCUBA, there had been some successful submillimetre observations of high redshift objects (Dunlop et al. 1994; Isaak et al. 1994; Ivison 1995) but interpretation of the measurements, particularly the high implied dust masses, was hampered by a lack of knowledge of local submillimetre properties, such as luminosity and dust mass functions (Eales & Edmunds 1996, 1997 hereafter EE96,97). We have started to use SCUBA to carry out a survey of a large number of nearby galaxies and hope that this first statistical submillimetre survey will answer a number of questions.

1.1 How much dust does a galaxy contain?

The amount of dust in a galaxy is a measure of the quantity of heavy elements in the interstellar medium (ISM), since ~ 50 per cent of the heavy elements are locked up in dust and there is some evidence that this fraction is constant from galaxy to galaxy (EE96). This is a different and complementary way of investigating the heavy element content from simply measuring the metallicity, which is of course, the mass of heavy elements *per unit mass* of gas not including that which is locked up in dust. EE96 have shown that the way in which the dust mass of a galaxy evolves depends critically on the mode of evolution:– whether the galaxy can be treated as a closed box or whether gas is inflowing onto or outflowing from it. Dust masses have been estimated from *IRAS* measurements but the resulting gas-to-dust ratios are a factor of ~ 5 – 10 higher than for our own Galaxy (Devereux & Young 1990; Sanders et al. 1991) suggesting a problem with the method. The submillimetre offers a number of advantages for estimating dust masses. At longer submillimetre wavelengths ($\lambda > 350\mu\text{m}$) we are sampling the Rayleigh-Jeans part of the Planck function, where the flux is least sensitive to temperature and most sensitive to the mass of the emitting material. This is a good thing because accurate dust temperatures (T_d) are difficult to estimate. Dust radiates as a ‘grey body’, which is a Planck

function modified by an emissivity term $Q_{em} \propto \nu^\beta$, where the emissivity index (β) is believed to lie between 1 and 2 (Hildebrand 1983). To derive the temperature, an assumption must be made about β or vice-versa. If an incorrect temperature is assumed at say $850\mu\text{m}$, then the dust mass will be wrong by approximately the fractional error in T_d , but at shorter FIR wavelengths ($100\mu\text{m}$) the error will be much larger as flux goes as $T_d^{(4+\beta)}$. Generally, using *IRAS* measurements alone to determine the temperature and mass will always over-estimate the first and so under-estimate the second. The reason for this is that because of the sensitivity to temperature of emission on the Wien side of the grey-body curve, the FIR emission from a galaxy is dominated by warm dust, even when there is relatively little mass in this component. Thus fits of grey-body curves to FIR fluxes are biased towards higher temperatures than is warranted by the relative masses of warm and cold dust. This is, of course, the probable explanation of the high gas-to-dust ratios observed by Devereux & Young (1990), and also explains why it has been so difficult to demonstrate the presence of cold dust in galaxies. Longer wavelength studies ($200\mu\text{m} - 850\mu\text{m}$) using *COBE*, *ISO* and SCUBA (Sodroski et al. 1994; Reach et al. 1995; Alton et al. 1998a,b; Davies et al. 1999; Frayer et al. 1999; Papadopoulos & Seaquist 1999) have now confirmed the existence of cold dust components at $15 < T_d < 25\text{ K}$ in nearby spiral galaxies as predicted for grains heated by the general interstellar radiation field (Cox, Krügel & Mezger 1986), rather than in star forming regions.

There is one further difficulty in estimating dust masses at any wavelength:– our poor knowledge of the dust mass opacity coefficient $\kappa_d(\nu)$, which is needed to give absolute values for mass. This varies with frequency in the same way as the emissivity, and so current measurements at 120 – $200\mu\text{m}$ (Hildebrand 1983, Draine & Lee 1984) must be extrapolated to the wavelength of interest using the assumed value of β , raising the possibility of large errors since β itself is poorly known. Hughes, Dunlop & Rawlings (1997) estimate the uncertainty in this coefficient to be a factor ~ 8 at $850\mu\text{m}$. For many issues, including galaxy evolution, absolute values of mass are not important (EE96) provided the relative masses are correct.

1.2 How much optical light is absorbed by dust?

There is an increasing need to understand the effects of dust on our optical view of the universe. Optical astronomers have recently shown that the UV luminosity density in the universe may rise from now to $z \sim 1$ and then fall off at higher redshifts (Lilly et al. 1996; Madau et al. 1996). There have been claims that this represents the ‘star-formation history of the universe’ but how much is this affected by dust? In general, how important are selection effects caused by dust, and is the high redshift universe significantly attenuated by foreground dusty objects? (Davies et al. 1997). Mapping large numbers of galaxies at submillimetre wavelengths will help determine how the dust is distributed relative to the stars, and how effective it is at absorbing optical light.

* The JCMT is operated by the Joint Astronomy Center on behalf of the UK Particle Physics and Astronomy Research Council, the Netherlands Organization for scientific Research and the Canadian National Research Council.

1.3 How much cosmological evolution is seen in the submillimetre?

With the deep SCUBA surveys now taking place (Smail, Ivison & Blain 1997; Hughes et al. 1998; Barger et al. 1998, 1999; Blain et al. 1999a; Eales et al. 1999; Lilly et al. 1999), there is now probably more information about the submillimetre properties of the distant universe than the local universe. The galaxies in the deep submillimetre surveys appear very similar to the ULIRGs found nearby (Smail et al. 1998; Hughes et al. 1998; Lilly et al. 1999). If the dust in these high-redshift objects is heated by young stars, as seems to be largely the case for nearby ULIRGs (Genzel et al. 1998) then, since these sources make up >20 per cent of the total extra-galactic background emission, this implies that ≥ 10 per cent of all the stars that have ever formed did so in this kind of extreme object (Eales et al. 1999). Studies of the cosmological evolution of this population suggests that it is very similar to that seen at optical wavelengths in the Lilly-Madau curve. What is derived for the cosmological evolution, however, depends critically on what is assumed about the submillimetre properties of the local universe (cf. results of Eales et al. 1999 and Blain et al. 1999b). Currently, rather than working from a local submillimetre luminosity function, most investigations have perforce started from a local *IRAS* $60\mu\text{m}$ luminosity function and extrapolated to submillimetre wavelengths using some assumptions about the average FIR-submm SED. The lack of a direct submillimetre luminosity function has been a severe limitation when interpreting the results of deep surveys. Even before SCUBA, submillimetre observations of high-redshift radio galaxies and quasars have found unusually high dust masses. Here again, explanation has been restricted by our ignorance of the local universe, in this case the statistics of dust masses in galaxies (EE 96).

1.4 Is CO a good tracer of molecular hydrogen?

Carbon monoxide (CO) has long been used as a tracer for molecular gas (H_2). The conversion factor between CO and H_2 (known as the ‘ X ’ factor) is quite uncertain and may be a function of physical environment such as density, temperature and metallicity (Maloney 1990; Wilson 1995). Dust is an alternative tracer of H_2 , and may help support the case for or against CO. Any variations of the ratio of CO to dust would provide insight on the way in which the X factor depends on galaxy properties.

1.5 The scope of the survey

The ideal way to carry out the survey would be to do a blank field survey of large parts of the sky and measure the redshifts of all objects detected, a method which would be largely free of any selection effects. Unfortunately, this is impractical at the moment because the field of view of SCUBA is only ~ 2 arcmins, making the time needed for such a survey prohibitively long. Instead, we decided to use the less ideal but more practical method of observing galaxies drawn from as many different complete samples selected in as many different wavebands as possible. This procedure

still allows us to produce unbiased estimates of the submillimetre luminosity function and of the dust mass function using ‘accessible volume’ techniques (Avni & Bahcall 1980). These will not be biased unless there is a class of galaxies which is not represented in any of the samples. Provided at least one member of such a class of objects is present in one of the samples then the estimates will be unbiased although clearly with large random errors.

In this paper we present the results from a sample selected at $60\mu\text{m}$. We present first estimates of the luminosity and dust mass functions, and examine the extent to which these may be biased. Subsequent papers on other samples, in particular a sample selected at optical wavelengths, will allow us to refine these estimates. We will also begin to address the other questions raised in this section.

Section 2 describes the observations and the methods used to reduce the data. In Section 3 we present the results from the *IRAS*-selected sample, in Section 4 we discuss the submillimetre luminosity and dust mass functions while in Section 5 we compare our results with other data (gas masses, optical properties) taken from the literature.

We assume a Hubble constant of $75 \text{ km s}^{-1} \text{ Mpc}^{-1}$ throughout.

2 OBSERVATIONS AND DATA REDUCTION

2.1 The Sample

The *IRAS*-selected sample was taken from the revised Bright Galaxy Sample (BGS), which is complete to a flux limit of $S_{60} > 5.24 \text{ Jy}$ at all $|b| > 30^\circ$ and $\delta > -30^\circ$ (Soifer et al. 1989). We observed a subset of this sample with SCUBA, consisting of all galaxies with declination from $-10^\circ < \delta < 50^\circ$ and with velocity $> 1900 \text{ km s}^{-1}$, a limit imposed to try to ensure the galaxies fitted within the SCUBA field of view. The SCUBA sample covers an area of $\approx 10,400 \text{ sq}^\circ$ and contains 104 objects. Many of these are interacting pairs and although most were resolved by SCUBA they were not by *IRAS*, even with subsequent HIRES processing (Surace et al. 1993). Table 1 lists the sample.

2.2 Observations

We observed the galaxies between July 1997 and September 1998 using the SCUBA bolometer array at the 15-m James Clerk Maxwell Telescope (JCMT) on Mauna Kea, Hawaii. SCUBA has two arrays of 37 and 91 bolometers for operation at long ($850\mu\text{m}$) and short ($450\mu\text{m}$) wavelengths respectively. They operate simultaneously with a field of view of ~ 2.3 arcmins (slightly smaller at $450\mu\text{m}$). The arrays are cooled to 0.1 K and have typical sensitivities (NEFDs) of $90 \text{ mJy Hz}^{-1/2}$ at $850\mu\text{m}$ and $700 \text{ mJy Hz}^{-1/2}$ at $450\mu\text{m}$ (Holland et al. 1999). Beam sizes were measured to be ~ 15 arcsec and 8 arcsec at 850 and $450\mu\text{m}$ respectively, depending on chop throw and conditions. We made our observations in ‘jiggle-map’ mode, which is the most efficient mapping mode for sources smaller than the field of view. The arrangement of the bolometers is such that the sky is instantaneously under-sampled and so the secondary mirror is stepped in a 16-point pattern to ‘fill in the gaps’. For observations using

both arrays, a 64 offset pattern is required to fully sample the sky as the spacing/size of the feedhorns is larger for the long wavelength array. Generally we used the 64-point jiggle, except in some cases where it was clear that the atmospheric conditions were too poor to obtain useful $450\mu\text{m}$ data, when we instead used the 16-point jiggle to give better sky cancellation.

The telescope has a chopping secondary mirror operating at 7.8 Hz which provides cancellation of rapid sky variations. To compensate for linear sky gradients (the effect of a gradual increase or decrease in sky brightness), the telescope is nodded to the ‘off’ position when in ‘jiggle’ mode. We used a chop throw of 120 arcsec in azimuth in all observations, except for galaxies with nearby companions, when we chose a chop direction which avoided the second galaxy. Skydips were performed regularly to measure the zenith opacity τ_{850} . This varied over the course of the observations resulting in some data being taken in excellent conditions with $\tau_{850} < 0.2$ while others done in ‘back-up’ mode had $\tau_{850} \sim 0.5\text{--}0.6$. Due to the large range of observing conditions, only about one third of the galaxies have useful $450\mu\text{m}$ data and, in fact, we will not consider the $450\mu\text{m}$ data further in this paper although they will be presented in another paper at a later date. We checked the pointing regularly and found it generally to be good to ~ 2 arcsec. Due to the uncertainty of the *IRAS* positions, we centred our observations on the optical coordinates taken from the *Digitised Sky Survey* (DSS)[†].

Integration times differed depending on conditions and source strength. For bright sources in good weather we typically used 6 integrations (15 mins), but many sources had to be observed on more than one occasion due to poor S/N or because the galaxy fell on noisy bolometers. In total we integrated for ~ 44 hours, mostly in weather band 3 ($0.3 \leq \tau_{850} \leq 0.5$). We calibrated our data by making jiggle maps of planets (Uranus and Mars) and, when they were unavailable, of the secondary calibrators CRL 618 and HL Tau. Planet fluxes were taken from the JCMT FLUXES program and we assumed that CRL 618 and HL Tau had fluxes of $4.56 \text{ Jy beam}^{-1}$ and $2.32 \text{ Jy beam}^{-1}$ respectively. The calibration error at $850\mu\text{m}$ was taken to be 10 per cent (except for 7 galaxies observed in very poor conditions where 15 per cent was used instead. These are denoted by a * in Table 1.). This calibration error is included in the flux error quoted in Table 1.

2.3 Data reduction

We reduced the data using the standard SURF package (Jenness & Lightfoot 1998). This consisted of flat-fielding the data after the on-off positions had been subtracted and then correcting for atmospheric extinction using opacities derived from skydip measurements. Any noisy bolometers were flagged as ‘bad’ and large spikes removed.

[†] The Digitised Sky Surveys were produced at the Space Telescope Science Institute under U.S. Government grant NAGW-2166. The images of these surveys are based on photographic data obtained using the Oschin Schmidt Telescope on Palomar Mountain and the U.K. Schmidt Telescope. The plates were processed into the present digital form with the permission of these institutions.

Table 1: Flux densities and SED parameters

(1)	(2)	(3)	(4)	(5)	(6)	(7)	(8)	(9)	(10)	(11)	(12)
Name	R.A. (J2000)	Decl. (J2000)	cz (km s ⁻¹)	S_{60} (Jy)	S_{100} (Jy)	S_{850} (mJy)	σ_{850} (mJy)	T_d (K)	$\sigma(T_d)$ (K)	β	$\sigma(\beta)$
NGC 23	0 09 53.4	+25 55 26	4565	8.77	14.96	144	25	34.4	3.0	1.3	0.2
UGC 556	0 54 50.3	+29 14 47	4629	5.36	9.99	79	15	32.0	2.6	1.5	0.2
NGC 470	1 19 44.8	+03 24 35	2374	7.09	12.01	213	30	38.0	3.0	0.9	0.2
MCG+02-04-025	1 20 02.7	+14 21 43	9362	10.72	9.60	39	8	44.6	4.6	1.4	0.2
UGC 903	1 21 47.9	+17 35 34	2518	7.91	14.58	178	26	34.4	3.1	1.2	0.2
NGC 520	1 24 34.9	+03 47 31	2281	31.55	46.56	325	50	36.2	3.1	1.4	0.2
III ZW 035	1 44 30.5	+17 06 08	8215	11.86	13.75	76	15	39.2	3.8	1.4	0.2
NGC 695	1 51 14.3	+22 34 56	9735	7.61	13.80	136	21	33.8	2.8	1.3	0.2
NGC 697	1 51 17.5	+22 21 30	3117	5.62	16.54	221	48*	27.8	2.2	1.5	0.2
UGC 1351	1 52 59.6	+12 42 31	4558	6.12	11.71	141	21	34.4	2.8	1.2	0.2
UGC 1451	1 58 30.0	+25 21 36	4916	6.75	12.20	107	18	33.2	2.6	1.4	0.2
NGC 772	1 59 19.5	+19 00 30	2472	6.78	24.11	288	43	25.4	1.7	1.7	0.2
NGC 877	2 17 59.5	+14 32 42	3913	11.76	23.34	332	43	34.4	2.8	1.1	0.2
NGC 958	2 30 42.8	-02 56 23	5738	5.90	14.99	262	34	30.8	2.0	1.2	0.2
NGC 992	2 37 25.5	+21 06 03	4141	10.96	15.63	146	26	38.0	3.5	1.2	0.2
UGC 2238	2 46 17.5	+13 05 48	6436	8.16	15.22	104	14	31.4	2.9	1.6	0.2
IR 0243+21	2 46 39.2	+21 35 11	6987	5.50	6.25	40	8	41.0	4.5	1.3	0.2
NGC 1134	2 53 41.5	+13 00 53	3651	8.99	16.07	242	31	36.2	3.4	1.0	0.2
UGC 2369	2 54 01.8	+14 58 14	9400	7.68	11.10	72	13	36.2	3.4	1.4	0.2
UGC 2403	2 55 57.2	+00 41 33	4161	7.51	11.77	111	18	36.8	2.9	1.2	0.2
NGC 1222	3 08 56.8	-02 57 18	2452	12.86	15.15	84	16	39.2	4.0	1.4	0.2
IR 0335+15	3 38 47.1	+15 32 53	10600	5.77	6.53	44	9	42.2	4.9	1.2	0.2
UGC 2982	4 12 22.5	+05 32 51	5305	8.70	17.32	176	34*	32.0	2.8	1.4	0.2
NGC 1614	4 34 00.0	-08 34 45	4778	33.12	36.19	219	32	41.6	4.2	1.3	0.2
NGC 1667	4 48 37.2	-06 19 12	4547	6.24	16.54	163	22	28.4	1.7	1.6	0.2
NGC 2623	8 38 24.1	+25 45 16	5535	25.72	27.36	91	14	39.8	4.1	1.6	0.2
IR 0857+39	9 00 24.5	+39 03 55	17480	7.66	5.06	17	7	50.6	9.0	1.4	0.4
NGC 2782	9 14 05.1	+40 06 49	2562	9.60	14.65	237	32	39.2	3.6	0.9	0.2
NGC 2785	9 15 15.4	+40 55 03	2734	9.21	16.78	201	33	34.4	3.1	1.2	0.2
UGC 4881	9 15 54.7	+44 19 52	11782	6.53	10.21	65	13	34.4	3.1	1.5	0.2
NGC 2856	9 24 16.2	+49 14 58	2638	6.15	10.28	89	16	35.0	2.9	1.3	0.2
MCG+08-18-012	9 36 37.2	+48 28 28	7777	6.39	8.83	42	10	35.6	3.4	1.6	0.2
NGC 2966	9 42 11.5	+04 40 23	2044	5.76	8.69	136	28	39.8	4.9	0.9	0.2
NGC 2990	9 46 17.2	+05 42 33	3088	5.49	10.16	110	19	33.8	3.2	1.3	0.2
IC 563/4 ^P	9 46 20.7	+03 03 31	6020	5.35	12.43	228	35	32.0	3.0	1.1	0.2
UGC 5376	10 00 26.8	+03 22 26	2050	5.94	11.49	148	23	33.8	2.9	1.2	0.2
NGC 3094	10 01 26.0	+15 46 13	2404	11.54	15.10	152	31	40.4	3.8	1.1	0.2
NGC 3110	10 04 02.0	-06 28 31	5048	11.68	23.16	188	28	32.0	2.3	1.5	0.2
IR 1017+08	10 20 00.2	+08 13 34	14390	6.08	5.97	36	6	44.0	4.3	1.2	0.2
NGC 3221	10 22 20.1	+21 34 09	4110	7.44	19.56	253	37	29.6	2.2	1.4	0.2
NGC 3367	10 46 34.6	+13 45 03	3037	6.06	12.49	132	21	31.4	2.6	1.4	0.2
IR 1056+24	10 59 18.2	+24 32 34	12912	12.53	16.06	61	13	35.6	3.3	1.7	0.2
ARP 148	11 03 54.0	+40 50 59	10350	6.95	10.99	92	20	35.6	3.0	1.3	0.2
NGC 3583	11 14 12.2	+48 18 56	2136	7.18	19.50	185	31	28.4	2.2	1.6	0.2
MCG+00-29-023	11 21 10.9	-02 59 13	7646	5.40	8.87	84	13	35.0	3.6	1.3	0.2
UGC 6436	11 25 46.6	+14 40 26	10243	5.60	9.80	106	18	35.0	3.2	1.2	0.2
NGC 3994/5 ^P	11 57 39.4	+32 17 08	3170	8.26	16.94	232	31	33.2	2.5	1.2	0.2
NGC 4045	12 02 42.2	+01 58 37	1981	6.50	13.57	142	25	31.4	2.6	1.4	0.2
IR 1211+03	12 13 46.1	+02 48 40	21703	8.39	9.10	49	10	42.2	5.2	1.3	0.2
NGC 4273	12 19 56.1	+05 20 37	2378	10.52	21.02	324	46	33.8	3.2	1.1	0.2
IR 1222-06	12 25 03.9	-06 40 53	7902	5.79	7.53	74	15	40.4	4.9	1.1	0.2
NGC 4418	12 26 54.7	-00 52 39	2179	42.32	30.76	255	37	55.4	8.0	0.9	0.2
NGC 4433	12 27 38.7	-08 16 42	3000	14.15	22.42	220	47	36.8	3.5	1.2	0.2
NGC 4793	12 54 41.1	+28 56 21	2484	12.49	27.99	258	42	30.2	2.5	1.5	0.2
NGC 4922	13 01 25.3	+29 18 49	7071	6.20	7.30	53	12	41.6	4.4	1.2	0.2

Table 1: ... continued

(1)	(2)	(3)	(4)	(5)	(6)	(7)	(8)	(9)	(10)	(11)	(12)
Name	R.A. (J2000)	Decl. (J2000)	cz (km s ⁻¹)	S_{60} (Jy)	S_{100} (Jy)	S_{850} (mJy)	σ_{850} (mJy)	T_d (K)	$\sigma(T_d)$ (K)	β	$\sigma(\beta)$
NGC 5020	13 12 39.8	+12 35 58	3362	5.39	10.01	206	34	36.2	3.1	0.9	0.2
IC 860	13 15 03.5	+24 37 08	3347	17.66	17.66	118	20	43.4	4.4	1.2	0.2
UGC 8387	13 20 35.3	+34 08 22	7000	13.69	24.90	113	15	30.8	2.4	1.8	0.2
NGC 5104	13 21 23.2	+00 20 32	5578	6.69	12.77	91	20*	31.4	2.9	1.6	0.2
NGC 5256	13 38 17.5	+48 16 36	8353	7.19	10.35	82	17	36.8	4.6	1.3	0.2
NGC 5257/8 ^P	13 39 55.5	+00 50 09	6770	10.68	20.80	283	39*	33.2	2.4	1.2	0.2
UGC 8739	13 49 14.0	+35 15 24	5032	5.90	14.32	187	27	30.8	2.4	1.3	0.2
NGC 5371	13 55 39.0	+40 27 31	2553	5.40	18.16	136	24	25.4	1.5	1.9	0.2
NGC 5394/5 ^P	13 58 38.1	+37 26 27	3470	9.07	21.51	269	36	30.2	2.6	1.4	0.2
NGC 5433	14 02 36.0	+32 30 38	4354	6.34	11.26	163	28	35.6	3.4	1.1	0.2
NGC 5426/7 ^P	14 03 26.0	-06 01 50	2678	9.93	24.81	548	86*	32.0	2.8	1.0	0.2
ZW 247.020	14 19 43.3	+49 14 12	7666	5.91	8.25	36	8	34.4	3.4	1.7	0.2
NGC 5600	14 23 49.2	+14 38 22	2319	5.35	11.46	112	22	31.4	2.6	1.4	0.2
NGC 5653	14 30 10.2	+31 12 56	3562	10.27	21.86	205	32	30.8	2.0	1.5	0.2
NGC 5665	14 32 25.9	+08 04 47	2228	6.18	11.67	157	27	35.0	3.4	1.1	0.2
NGC 5676	14 32 46.7	+49 27 29	2114	12.00	29.78	481	69	30.8	1.8	1.2	0.2
NGC 5713	14 40 11.4	-00 17 26	1900	20.69	36.27	359	44	34.4	3.1	1.3	0.2
UGC 9618 ^P	14 57 00.5	+24 36 42	9900	6.68	14.54	215	31	32.0	2.6	1.2	0.2
NGC 5792	14 58 22.7	-01 05 29	1924	9.45	18.31	383	56	35.6	3.2	0.9	0.2
ZW 049.057	15 13 13.1	+07 13 31	3927	21.06	29.88	200	27	36.2	3.2	1.4	0.2
NGC 5900	15 15 05.2	+42 12 36	2511	7.36	16.69	179	23	30.8	2.6	1.4	0.2
1 Zw 107	15 18 06.1	+42 44 45	11946	9.15	10.04	60	14	41.6	4.6	1.3	0.2
NGC 5929/30 ^P	15 26 06.3	+41 40 24	2617	9.14	13.69	119	22	36.2	3.1	1.3	0.2
IR 1525+36	15 26 59.4	+35 58 37	16009	7.20	5.78	43	10	50.6	6.9	1.0	0.2
NGC 5936	15 30 00.9	+12 59 21	4004	8.56	16.84	152	28	32.6	2.9	1.4	0.2
NGC 5937	15 30 46.1	-02 49 46	2758	10.23	20.56	247	39	32.6	2.7	1.3	0.2
NGC 5953/4 ^P	15 34 33.7	+15 11 50	1960	11.55	19.50	306	31	36.8	4.1	1.0	0.2
ARP 220	15 34 57.2	+23 30 11	5452	103.33	113.95	832	86	42.2	5.7	1.2	0.2
IR 1533-05	15 36 11.7	-05 23 52	8186	5.25	8.96	79	15	35.0	3.0	1.3	0.2
NGC 5962	15 36 32.0	+16 36 22	1963	8.99	20.79	317	37	32.0	2.7	1.2	0.2
NGC 5990	15 46 16.4	+02 24 55	3839	9.20	15.46	110	23	33.2	2.7	1.5	0.2
NGC 6052	16 05 13.0	+20 32 34	4712	6.46	10.18	95	15	35.6	3.5	1.3	0.2
MCG+01-42-008	16 30 56.5	+04 04 58	7342	7.38	12.48	95	18	34.4	2.8	1.4	0.2
NGC 6181	16 32 21.2	+19 49 30	2379	9.35	21.00	228	37	30.8	2.6	1.4	0.2
NGC 7448	23 00 03.6	+15 58 56	2192	8.32	17.08	193	32	32.6	2.8	1.3	0.2
NGC 7469 ^P	23 03 16.4	+08 52 50	4892	27.68	34.91	264	30	40.4	3.9	1.2	0.2
NGC 7479	23 04 56.5	+12 19 19	2381	15.35	24.60	335	56	38.0	3.8	1.0	0.2
ZW 453.062	23 04 56.5	+19 33 08	7524	7.06	10.39	69	14	36.2	3.5	1.4	0.2
NGC 7541	23 14 43.4	+04 32 04	2665	20.59	40.63	427	60	33.2	2.4	1.3	0.2
ZW 475.056	23 16 00.6	+25 33 25	8197	8.75	11.64	77	15	37.4	3.8	1.4	0.2
NGC 7591	23 18 16.3	+06 35 10	4956	7.82	13.52	135	21	34.4	2.8	1.3	0.2
NGC 7592	23 18 22.1	-04 24 58	7350	8.02	10.50	108	19	39.8	3.8	1.1	0.2
NGC 7674	23 27 56.7	+08 46 44	8713	5.28	7.91	108	20	38.6	4.2	1.0	0.2
NGC 7678	23 28 26.2	+22 25 02	3489	7.01	14.84	195	26	33.2	2.7	1.2	0.2
NGC 7679	23 28 46.7	+03 30 41	5138	7.28	10.65	93	15	38.0	3.6	1.2	0.2
NGC 7714	23 36 14.1	+02 09 18	2798	10.52	11.66	72	13	41.0	6.9	1.3	0.2
NGC 7771	23 51 24.9	+20 06 42	4256	20.46	37.42	377	42	33.8	3.0	1.3	0.2
MRK 331	23 51 26.8	+20 35 10	5541	17.32	20.86	132	25	40.4	4.3	1.3	0.2
UGC 12914/5 ^P	00 01 39.6	+23 29 33	4350	6.27	13.40	191	30	32.6	2.6	1.2	0.2

Notes to Table 1:

(1) Most commonly used name taken from the IRAS BGS
 (2) Right ascension J2000 epoch (3) Declination J2000 epoch
 (4) Recession velocity taken from NED[‡] (5) 60 μ m flux from
 Soifer et al. 1989 (7) 850 μ m flux (this work) (8) error on
 850 μ m flux, calculated in the manner described in Section
 2.4 and inclusive of a 10% calibration uncertainty. A * indi-
 cates that a 15% calibration uncertainty was used. (9) Dust
 temperature derived from a single component fit to the 60,
 100 and 850 μ m data points as described in Section 3.1 (10)
 Statistical uncertainty in the dust temperature as described
 in Section 3.1 (11) Emissivity index derived from the single
 component fit, described in Section 3.1 (12) Statistical un-
 certainty in the emissivity index as described in Section 3.1
^p indicates a close or interacting pair which was resolved by
 SCUBA. Individual fluxes are listed in Table 2.

Except on the most dry and stable nights a residual sky
 noise was seen which was correlated across all the pixels.
 In most cases we removed this using the SURF task REM-
 SKY, which uses bolometers chosen by the user to define a
 sky region, and then subtracts this sky level from the other
 bolometers. The bolometers used to measure the ‘sky’ were
 chosen to be those away from the source emission using a
 rough submillimetre map and optical information as a guide.
 After sky noise removal, the data was despiked and regrid-
 ded to form an image on 1 arcsec pixels. If an object had
 more than one dataset, a co-add was made in which each
 map was weighted as the inverse square of its measured
 noise.

The nodding and chopping should ideally leave a back-
 ground with zero mean and some correlated noise superim-
 posed on top. In reality the background level was not zero
 and could, in bad conditions, become quite large (either pos-
 itive or negative). Often this residual sky level would vary
 linearly across the array giving a ‘tilted sky plane’, the SURF
 task REMSKY, which was designed to remove the sky noise is
 rather simplistic and cannot remove these sky planes (Jen-
 ness, Lightfoot & Holland 1998). Due to the short integra-
 tion times of most of our objects and the poor conditions in
 which many were observed, this problem of sky planes be-
 came the limiting factor in obtaining sufficient S/N in many
 observations. To this end a program was written to remove
 spatially varying sky backgrounds from the array as well as
 the temporal ‘sky noise’ dealt with by REMSKY.

Two fairly typical 850 μ m images are shown in Figure 1
 along with optical images from the DSS. The SCUBA im-
 ages clearly contain large amounts of structural information,
 which we will delay considering until a later paper. Here we
 will simply consider the 850 μ m flux measurements.

2.4 Flux measurement and error analysis

We used the submillimetre images to choose an aperture
 over which to integrate the flux, trying to ensure that it

contained all the flux associated with the galaxy and as lit-
 tle of the surrounding sky as possible.

The noise /error on the flux measurement has two com-
 ponents.

i) The error in subtracting the background sky level
 which, despite our best attempts at removing it, often had
 a non-zero value that varied over the image. A number
 of smaller apertures were placed on regions containing no
 source emission and used to estimate the mean sky level.
 The standard deviation between the sky levels in each aper-
 ture was then used to find the error in the mean sky as
 $\sigma_{ms} = S.D./\sqrt{No.aps}$, where ‘No. aps’ is the number of
 sky apertures used to determine the mean sky value. The
 noise in the object aperture due to this sky error is then
 $\sigma_{sky} = \sigma_{ms}N_{ap}$ where N_{ap} is the number of pixels in the
 object aperture.

ii) Shot/Poisson noise from pixel to pixel variations
 within the sky aperture, which would usually be deter-
 mined from the standard deviation of the pixels within the
 sky aperture and contribute to the flux error as $\sigma_{shot} =$
 $\sigma_{pix} \sqrt{N_{ap}}$. In ordinary CCD astronomy this would be the
 only error estimated and we will refer to it as the ‘theoretical
 error’. It is actually quite a large underestimate of the true
 shot noise because the noise is correlated across pixels. This
 is because, unlike a CCD image, the pixels of a SCUBA
 image do not contain independent samples of the sky, i.e.
 two neighbouring pixels on a SCUBA image are constructed
 from overlapping sets of bolometer measurements, (also the
 pixels on the SCUBA maps are ‘artificial’ as they are smaller
 than the size of the beam). To quantify this effect, simula-
 tions of blank SCUBA fields were made by replacing the
 data for each bolometer in an observation by the output
 of a Gaussian random number generator. A large number
 of artificial maps were made in this way, and on each map
 the noise in an aperture of given size was measured in the
 traditional way using $\sigma_{shot} = \sigma_{pix} \sqrt{N_{ap}}$. This was com-
 pared with the standard deviation of all the fluxes (in that
 size aperture) between the different maps, deemed to be the
 ‘real shot noise’. For the range of aperture sizes actually used
 in measuring fluxes, the ratio of real to predicted noise was
 ~ 8 . The total error for each flux was calculated from

$$\sigma_{tot} = (\sigma_{cal}^2 + \sigma_{sky}^2 + \sigma_{shot}^2)^{1/2}$$

$$\text{where } \sigma_{cal} \approx 10\%$$

$$\sigma_{sky} = \sigma_{ms}N_{ap}$$

$$\sigma_{shot} = 8 \sigma_{pix} \sqrt{N_{ap}}$$

To convert the aperture flux in volts to Janskys, a mea-
 surement of the calibrator flux for that night was made using
 the same aperture as was used for the object. The orien-
 tation of the aperture relative to the chop throw was also
 translated to the calibrator map (this did have a significant
 effect for more elliptical apertures).

Fluxes were found to have total errors σ_{tot} in the range
 10–25 per cent at 850 μ m and these are listed in Table 1.
 All objects were detected at $> 3\sigma$ except for IR 0857+39,
 which was only detected at 2.4σ , although the flux is in good

[‡] The NASA/IPAC Extragalactic Database (NED) is operated
 by the Jet Propulsion Laboratory, California Institute of Tech-
 nology, under contract with the National Aeronautics and Space
 Administration.

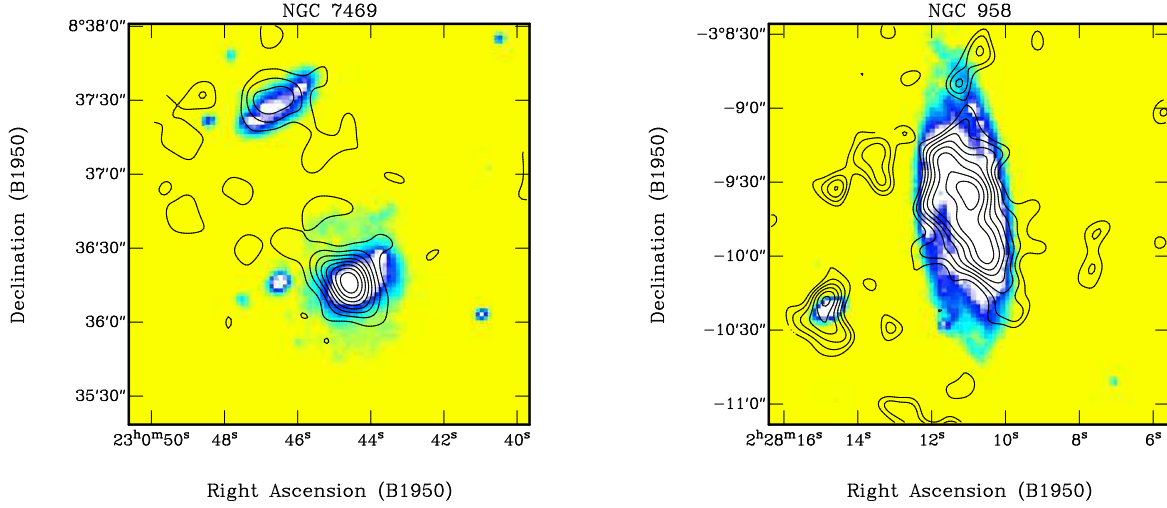


Figure 1. a) SCUBA contours (2, 4, 6... σ) overlaid on an optical DSS image for the Seyfert 1 galaxy NGC 7469 (lower), and its companion IC 5283. There appears to be extended emission between the two galaxies. b) SCUBA contours (2, 3, 4... σ) overlaid over the optical DSS image for NGC 958. The companion satellite ~ 1 arcmin to the east is a surprise detection (~ 35 mJy) as it has no 1.49 GHz flux.

Table 2. Fluxes for pairs resolved by SCUBA

Name	R.A. (J2000)	Decl. (J2000)	<i>cz</i> (km s ⁻¹)	<i>S</i> ₆₀ (Jy)	<i>S</i> ₁₀₀ (Jy)	<i>S</i> ₈₅₀ (mJy)	σ_{850} (mJy)	<i>T</i> _d (K)	$\sigma(T_d)$ (K)	β	$\sigma(\beta)$
IC 563	9 46 20.3	+03 02 46	6093	^h 2.90	^h 5.87	103	24	34.4	2.7	1.0	0.2
IC 564	9 46 21.0	+03 04 19	6026	^h 2.46	^h 6.56	125	26	30.8	2.0	1.1	0.2
NGC 3994	11 57 36.9	+32 16 38	3096	^h 5.00	^h 10.31	106	20	32.0	2.3	1.4	0.2
NGC 3995	11 57 44.0	+32 17 37	3254	^h 3.27	^h 6.63	126	24	34.4	3.1	1.0	0.2
NGC 5257	13 39 52.1	+00 50 27	6798	U	U	114	23		
NGC 5258	13 39 57.4	+00 49 51	6757	U	U	169	32		
NGC 5394	13 58 33.7	+37 27 13	3451	U	U	71	17		
NGC 5395	13 58 37.6	+37 25 42	3491	U	U	198	32		
NGC 5426	14 03 24.7	-06 04 13	2621	^h 3.06	^h 8.50	287	63	32.0	2.6	0.8	0.2
NGC 5427	14 03 26.0	-06 01 50	2730	^h 6.87	^h 16.31	261	59	31.4	2.8	1.2	0.3
UGC 9618 (N)	14 57 00.7	+24 36 58	10094	U	U	135	24		
UGC 9618 (S)	14 57 00.0	+24 36 20	9776	U	U	80	20		
NGC 5929	15 26 06.1	+41 40 15	2561	U	U	~ 24	12		
NGC 5930	15 26 07.9	+41 40 34	2672	U	U	95	18		
NGC 5953	15 34 32.4	+15 11 40	1965	U	U	182	23		
NGC 5954	15 34 35.1	+15 12 04	1959	U	U	124	21		
NGC 7469	23 03 15.6	+08 52 29	4916	U	U	192	27		
IC 5283	23 03 18.2	+08 53 36	4894	U	U	72	12		
UGC 12914	00 01 38.3	+23 29 02	4371	U	U	131	22		
UGC 12915	00 01 42.1	+23 29 23	4336	U	U	160	21		

NOTES – *h* :- *IRAS* fluxes resolved using HIRES (Surace et al 1993), U :- unresolved by *IRAS*. Columns have the same meanings as Table 1

agreement with that measured by Rigopoulou et al. (1996). Where the system is interacting and not resolved by *IRAS*, the 850 μ m fluxes given are for both galaxies combined. For those paired galaxies which were resolved by SCUBA, the individual fluxes are listed in Table 2.

A few objects were detected with good signal to noise on more than one occasion and these could be used to keep check on the consistency of our flux measuring and calibration procedures. These objects and their relative flux errors

are detailed in Table 3 and it can be seen that the differences in measured fluxes are within the errors calculated in the manner described above.

3 RESULTS

Table 3. Galaxies with repeat flux measurements and their errors

(1) Object	(2) Date	(3) Ints.	(4) Weather (τ_{850})	(5) % error on individual observations Theoretical noise	(6) ‘True’ noise	(7) Actual difference %
Arp 220	2.7.97	5	0.2	0.3 (10.0)	2.6 (10.3)	1.7
	5.3.98	4	0.2	0.3 (10.0)	3.0 (10.4)	
NGC 1134	7.8.97	10	0.3	0.9 (10.0)	8.8 (13.3)	5.0
	7.8.97	10	0.3	1.1 (10.1)	11.6 (15.3)	
UGC 2238	14.8.97	10	0.4–0.5	1.9 (10.2)	15.7 (18.6)	13.3
	25.8.97	10	0.4–0.5	1.3 (10.1)	11.0 (14.9)	
UGC 903	14.8.97	10	0.4–0.5	1.2 (10.1)	10.6 (14.6)	10.6
	7.10.98	6	0.2	1.0 (10.0)	8.3 (13.0)	

(1) Galaxy name. (2) Date of each observation. (3) Number of integrations in observation. (4) Weather in terms of $850\mu\text{m}$ opacity. (5) The ‘theoretical’ noise on the individual observations, equivalent to shot noise on a CCD. Brackets give the error inclusive of 10% calibration uncertainty. (6) The ‘true’ noise on the individual observations, consisting of σ_{sky} and the ‘real’ σ_{shot} as described in Section 2.4, brackets again give error inclusive of 10% calibration uncertainty. (7) The actual percentage difference between the fluxes for both observations.

3.1 Spectral fits

We have fitted the *IRAS* 60, 100 and $850\mu\text{m}$ fluxes with a single-component temperature model by minimising the sum of the chi-squared residuals. The best fit was found for both the emissivity index β and temperature T_d , with the values given in Table 1. Some examples of fits are shown in Fig. 2 along with the 1σ ranges. The uncertainty of each fitted value of T_d and β was estimated in the following way. For each galaxy, a Gaussian random number generator was used to create 100 artificial flux sets from the original fluxes and measurement errors. These new data sets were then fitted in the same way and the standard deviation in the new parameters found from the real data set. Average values and standard deviations (S.D.) for the whole sample (i.e. using only the best fitting parameters for the real data sets) are $\overline{T_d} = 35.6 \pm 4.9$ K and $\overline{\beta} = 1.3 \pm 0.2$.

The value of β is remarkably uniform (the overall S.D. for the whole sample is of the same order as the individual uncertainties, derived from the above technique), and lower than the value of 1.5–2.0 obtained from multi-wavelength studies of our Galaxy (Masi et al. 1995; Reach et al. 1995), and also of NGC 891 (Alton et al. 1998b). The number of galaxies at $\beta \geq 1.5$ is equivalent to those at $\beta \leq 1.1$, and in fact, the distribution of β about the mean is well represented by a Gaussian, with those galaxies at $\beta > 1.5$ being the tail of that Gaussian. The distribution of β values for the sample is shown in Fig. 3. In fact, when the fluxes of the Milky Way and NGC 891 are fitted in the same way as we have fitted the *IRAS* galaxies (i.e. a single temperature model using only the 60, 100 and $850\mu\text{m}$ points) the β value we find is 0.7. It is only when the full SED is used (which includes fluxes between 200 and $800\mu\text{m}$) that the colder component at < 20 K can be identified, leading to the higher β of 1.5–2. So rather than implying that β truly does have a low value, our results probably indicate that there is dust in these galaxies at colder temperatures than is indicated by a single-component fit. The uniformity of the β values in

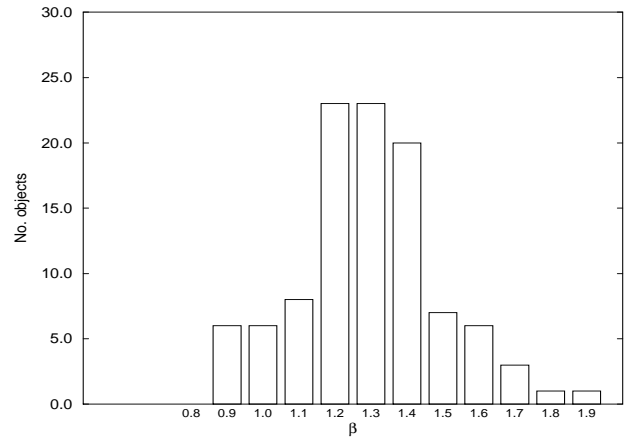


Figure 3. The distribution of β values for the sample, note that the value determined for the Galaxy with a multi-component model is 1.5–2.0

the sample could be indicative of similar cold component properties in all of the *IRAS* galaxies.

The lower β of 0.7 determined in this way for the Milky Way and NGC 891, which are optically selected, may be due to them having larger fractions of colder dust than the *IRAS* galaxies. We can partially test this using preliminary data from the optically selected sample. Figure 4 shows a colour-colour plot for the *IRAS* galaxies (stars) plus the galaxies observed so far from the optical sample (circles). There is clear evidence that the optically selected galaxies occupy a different area of the space, implying that they are not merely the less luminous equivalent of *IRAS* galaxies. We can make a more thorough investigation when the optically selected sample is completed and we have 350 and $450\mu\text{m}$ data for the samples.

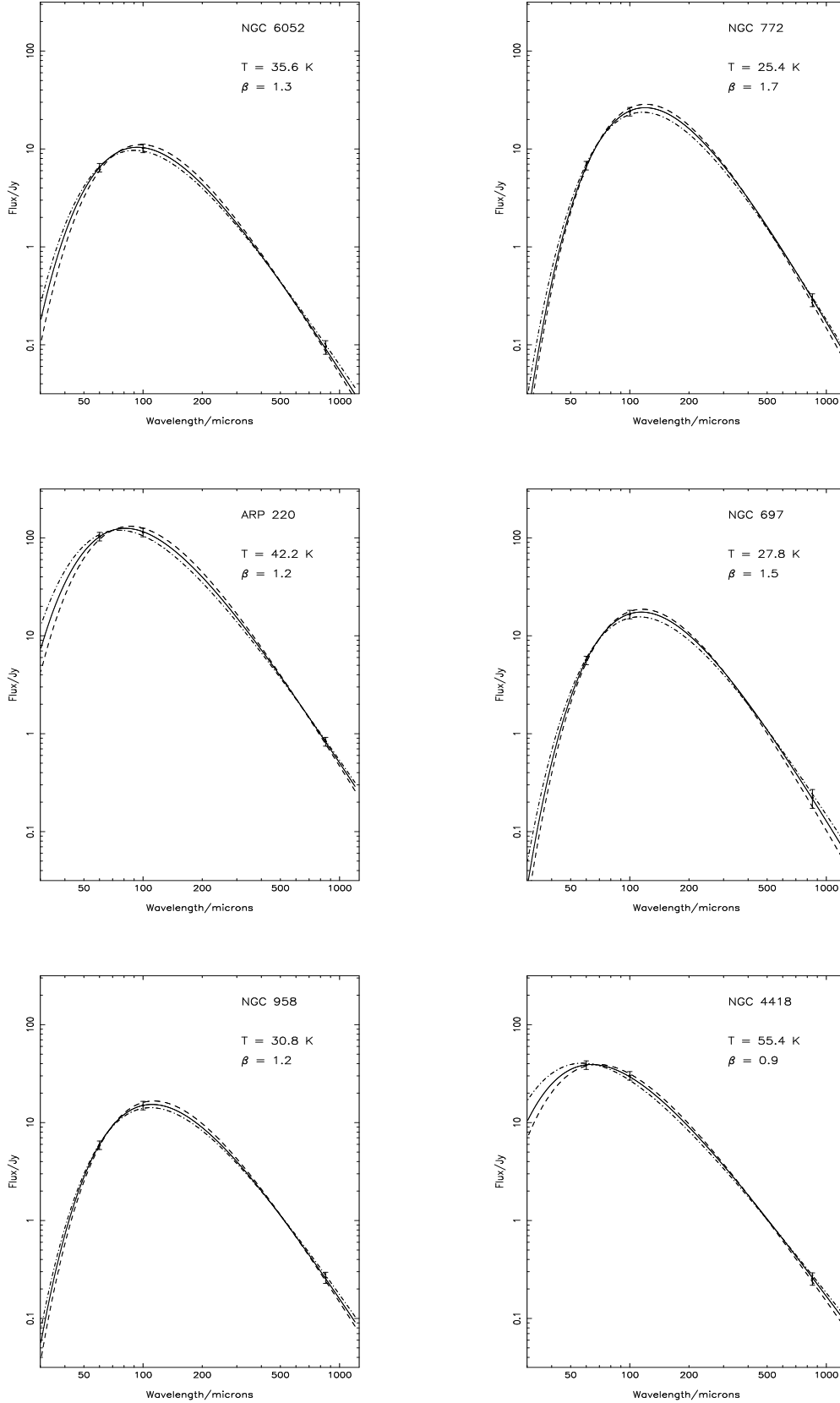


Figure 2. Representative SEDs showing the range of β and T_d for the sample. Data points are the 60 and 100 μ m *IRAS* fluxes and the 850 μ m point is from our survey 10 . The solid lines are the best-fitting lines relating to the SED parameters shown. The dashed and dot-dashed lines are the $\pm 1\sigma$ fits.

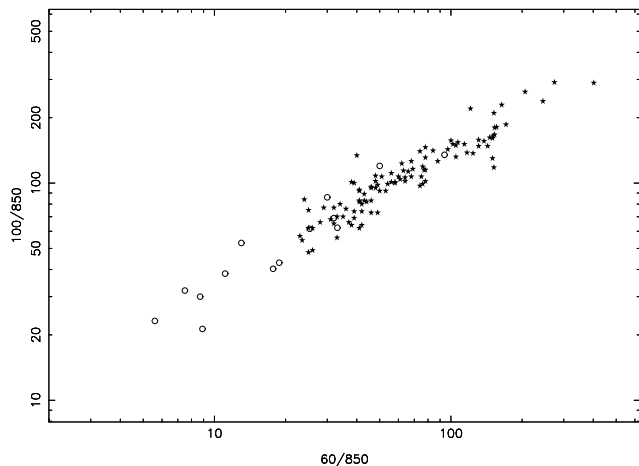


Figure 4. A plot of the 100/850 versus 60/850 colours for the *IRAS* sample described in this paper (solid symbols) plus the optically selected galaxies observed so far (open symbols). The two samples clearly have different FIR-submm properties.

3.2 Dust masses

Using the 850 μ m flux and the temperature derived in the above way the dust mass is calculated from

$$M_d = \frac{S_{850} D^2}{\kappa_d(\nu) B(\nu, T_d)} \quad (1)$$

where $\kappa_d(\nu)$ is the dust mass opacity coefficient, $B(\nu, T_d)$ is the value of the Planck function at 850 μ m for a temperature T_d , and D for $\Omega_0 = 1$ is given by

$$D = \frac{2c}{H_0} \left(1 - \frac{1}{\sqrt{1+z}} \right) \quad (2)$$

The dust masses are listed in Table 4, with values for individual members of pairs in Table 5. We have assumed a value of 0.077 m² kg⁻¹ for $\kappa_d(\nu)$, which is intermediate between values for graphite and silicates as given by Draine & Lee (1984) and by Hughes et al. (1993), and also that $\kappa_d(\nu)$ has the same value at 850 μ m for all our galaxies. Even though the value of $\kappa_d(\nu)$ is notoriously uncertain, the relative values of our dust masses will be correct as long as the dust has similar properties in all galaxies. The uncertainties in the relative dust masses then depend only on the errors in S_{850} and T_d . The formal statistical uncertainties in T_d are only \sim a few K, but there is the possibility that our assumption of a single temperature has biased our estimates of T_d to higher values, and thus our mass estimates to lower values. We can estimate the size of this effect in the following way: A single temperature fit will produce a lower value for β than is actually true if more than one component is present. In their *COBE*-FIRAS study of our Galaxy, Reach et al. (1995) concluded that the highest observed value of β in any region was likely to be closest to the true value, with any excess emission in other regions due to a colder component. If we adopt the same approach and assume that all our galaxies have a true β of 2 (our highest observed value is 1.9) and a uniform cold dust temperature of 20 K, we can then fit a two-component temperature model and calculate a new dust mass. We find that for the same mass coefficient as before, the masses of dust estimated from this two-component model are between 1.5 and 3 times higher than those derived

from a single temperature fit. The discrepancy is larger for galaxies with lower β and higher temperatures and some galaxies which have steep SEDs and cold temperatures have little extra dust when modelled in this way (e.g. NGC 5371, NGC 772). The dust masses calculated assuming this form for the cold component are listed alongside the single temperature masses in Table 4. They will be referred to as ‘cold dust masses’ in future.

3.3 Gas masses

Neutral hydrogen (HI) fluxes were taken from the literature[§] and converted to masses (in solar units) using

$$M_{\text{HI}} = 2.36 \times 10^5 D^2 S_{\text{HI}} \quad (3)$$

where D^2 (Eqn. 2) is in Mpc and S_{HI} is in Jy km s⁻¹

Molecular gas (H₂) masses were calculated using CO fluxes taken from the literature³ and scaled to telescope independent units (Jy km s⁻¹). When an object appeared in more than one reference, an average flux was used to determine the mass. Conversion factors used for different telescopes are given in Table 6. Molecular masses in M_\odot are given by

$$M_{\text{H}_2} = 1.1 \times 10^4 D^2 S_{\text{CO}} \quad (4)$$

(Kenny & Young 1989), in which the parameters have the same units as in Eqn. 3. This assumes a CO to H₂ conversion factor of $X = 2.8 \times 10^{20}$ H₂ cm⁻²/[K(T_R)km s⁻¹]. Atomic and molecular gas masses are also given in Table 4.

3.4 Optical luminosities

Blue magnitudes were taken from the Lyon-Meudon Extragalactic Database (LEDa) and converted to luminosities using $M_{B\odot} = 5.48$. Blue luminosities are given in Table 4 and are corrected for Galactic extinction but not for internal extinction or inclination effects. In future discussions involving L_B , mention will be made of ‘corrected’ blue luminosities. This will refer to the values in Table 4 after further correction for the internal effects of dust in the galaxy, and for inclination, following the prescription given in the 3rd Reference Catalogue of Bright Galaxies (RC3) (de Vaucouleurs et al. 1991).

3.5 Far Infra-Red Luminosities

The FIR luminosity (L_{fir}) is usually calculated using the 60 and 100 μ m *IRAS* fluxes, as described in the Appendix of *Catalogued Galaxies and Quasars Observed in the IRAS Survey* (Version 2, 1989):

$$\text{FIR} = 1.26 \times 10^{-14} (2.58 S_{60} + S_{100})$$

and

$$L_{\text{fir}} = 4\pi D^2 \times \text{FIR} \times C$$

[§] See notes to Table 4

Table 4: Luminosities and masses

Name	$\log L_{60}$ (W Hz ⁻¹ sr ⁻¹)	$\log L_{850}$ (W Hz ⁻¹ sr ⁻¹)	$\log L_{\text{fir}}$ (L _⊙)	$\log M_{\text{d}}$ (M _⊙)	$\log M_{\text{d}}^{\text{cold}}$ (M _⊙)	$\log M_{\text{HI}}$ (M _⊙)	$\log M_{\text{H}_2}$ (M _⊙)	$\log L_{\text{B}}$ (L _⊙)	G_{d}	$L_{\text{fir}}/M_{\text{H}_2}$ (L _⊙ /M _⊙)
	(1)	(2)	(3)	(4)	(5)	(6)	(7)	(8)	(9)	(10)
NGC 23	23.51	21.68	10.82	7.49	7.79	9.88	9.95	10.73	746	7.5
UGC 556	23.31	21.43	10.86	7.28	7.57	9.64	9.61	9.72	444	10.9
NGC 470	23.32	21.30	10.16	7.05	7.43	9.61	9.29	10.30	536	7.4
MCG+02-04-025	24.21	21.71	11.38	7.39	7.76	9.54	...	10.40
UGC 903	22.94	21.27	10.27	7.08	7.38	9.52	...	9.44
NGC 520	23.45	21.45	10.73	7.22	7.53	9.77	9.88	10.35	809	7.0
III ZW 035	24.15	21.90	11.36	7.64	7.96	9.36	9.90	9.97	238	28.6
NGC 695	24.12	22.29	11.42	8.11	8.41	10.33	10.55	10.86	443	7.8
NGC 697	22.98	21.55	10.49	7.47	7.66	10.37	...	10.43
UGC 1351	23.35	21.67	10.68	7.48	7.79	9.79	...	10.24
UGC 1451	23.46	21.62	10.78	7.44	7.71	9.63	...	10.11
NGC 772	22.86	21.46	10.46	7.44	7.56	10.36	10.15	10.81	1344	2.0
NGC 877	23.50	21.92	10.85	7.72	8.04	10.31	10.00	10.67	573	7.2
NGC 958	23.54	22.14	10.97	8.01	8.27	10.59	10.21	10.75	544	5.8
NGC 992	23.51	21.61	10.78	7.36	7.72	10.07	9.83	9.58	809	8.8
UGC 2238	23.78	21.83	11.11	7.69	7.90	10.02	10.22	10.20	550	7.9
IR 0243+21	23.67	21.48	10.88	7.20	7.58	9.13
NGC 1134	23.32	21.72	10.65	7.50	7.85	10.28	...	10.34
UGC 2369	24.09	21.98	11.33	7.77	8.07	10.49
UGC 2403	23.36	21.49	10.64	7.26	7.60	9.82
NGC 1222	23.12	20.92	10.36	6.66	6.98	9.38	...	9.98
IR 0335+15	24.06	21.87	11.25	7.57	7.98	...	10.44	9.95	...	6.4
UGC 2982	23.64	21.90	10.99	7.74	8.00	10.07	10.23	9.98	520	5.8
NGC 1614	24.12	21.90	11.33	7.61	8.00	9.54	10.09	10.34	389	17.2
NGC 1667	23.36	21.73	10.81	7.65	7.82	9.75	9.98	10.50	342	6.7
NGC 2623	24.13	21.66	11.33	7.39	7.67	9.25	9.97	10.32	456	22.7
IR 0857+39	24.55	21.85	11.68	7.46	8.00	...	9.69	11.12	...	98.0
NGC 2782	23.04	21.41	10.34	7.14	7.54	9.62	9.36	10.45	465	9.5
NGC 2785	23.08	21.39	10.42	7.20	7.51	8.99	...	9.42
UGC 4881	24.22	22.12	11.50	7.94	8.21	10.25	10.65	10.68	723	6.6
NGC 2856	22.87	21.01	10.18	6.80	7.11	9.15
MCG+08-18-012	23.84	21.59	11.07	7.38	7.65	10.21
NGC 2966	22.62	20.97	9.91	6.70	7.10	9.14	...	9.63
NGC 2990	22.96	21.23	10.30	7.05	7.35	9.69	...	10.05
IC 563/4	23.54	22.11	10.95	7.96	8.25	10.10	...	10.53
UGC 5376	22.63	21.01	10.00	6.83	7.13	9.41	...	9.54
NGC 3094	23.06	21.16	10.31	6.88	7.27	9.35	...	9.99
NGC 3110	23.72	21.88	11.06	7.73	7.98	...	10.34	10.52	...	5.2
IR 1017+08	24.35	22.03	11.52	7.71	8.16	...	10.38	13.8
NGC 3221	23.35	21.84	10.79	7.73	7.96	10.33	9.99	10.14	581	6.3
NGC 3367	22.99	21.30	10.38	7.16	7.40	9.77	...	10.68
IR 1056+24	24.58	22.16	11.78	7.96	8.18	...	10.36	10.92	...	26.2
ARP 148	24.13	22.17	11.39	7.96	8.32	...	10.21	15.4
NGC 3583	22.96	21.14	10.22	7.06	7.23	9.68	9.49	10.49	694	5.3
MCG+00-20-023	23.75	21.88	11.04	7.68	7.99	10.38
UGC 6436	24.03	22.23	11.32	8.02	8.36	9.88	10.30	10.45	260	10.5
NGC 3994/5	23.16	21.58	10.53	7.41	7.70	10.25	...	10.65
NGC 4045	22.64	20.97	10.04	6.82	7.07	9.13	...	10.02
IR 1211+03	24.86	22.48	12.00	8.19	8.60	...	10.64	10.47	...	22.9
NGC 4273	23.01	21.48	10.39	7.30	7.61	9.64	9.63	10.37	435	5.8
IR 1222-06	23.80	21.86	11.04	7.58	7.98	9.84
NGC 4418	23.50	21.30	10.68	6.86	7.41	8.75	9.12	9.68	261	36.4
NGC 4433	23.34	21.51	10.64	7.28	7.62	9.86	9.63	10.20	600	10.2
NGC 4793	23.12	21.42	10.54	7.30	7.51	9.79	9.67	10.41	550	7.4
NGC 4922	23.73	21.62	10.95	7.32	7.73	9.15	...	10.67

Table 4: ... continued

Name	$\log L_{60}$ (W Hz ⁻¹ sr ⁻¹)	$\log L_{850}$ (W Hz ⁻¹ sr ⁻¹)	$\log L_{\text{fir}}$ (L _⊙)	$\log M_{\text{d}}$ (M _⊙)	$\log M_{\text{d}}^{\text{cold}}$ (M _⊙)	$\log M_{\text{HI}}$ (M _⊙)	$\log M_{\text{H}_2}$ (M _⊙)	$\log L_{\text{B}}$ (L _⊙)	G_{d}	$L_{\text{fir}}/M_{\text{H}_2}$ (L _⊙ /M _⊙)
	(1)	(2)	(3)	(4)	(5)	(6)	(7)	(8)	(9)	(10)
NGC 5020	23.03	21.58	10.38	7.36	7.71	10.07	...	10.44
IC 860	23.51	21.33	10.72	7.01	7.43	...	8.91	9.68	...	64.1
UGC 8387	24.08	21.93	11.39	7.81	7.96	...	10.17	10.35	...	16.5
NGC 5104	23.57	21.65	10.90	7.51	7.74	9.83	...	10.34
NGC 5256	23.95	21.94	11.20	7.72	8.04	...	10.36	10.87	...	6.9
NGC 5257/8	23.94	22.31	11.24	8.14	8.44	10.55	...	11.04
UGC 8739	23.43	21.88	10.84	7.75	8.00	10.12	...	10.47
NGC 5371	22.79	21.16	10.34	7.14	7.18	10.05	...	10.80
NGC 5394/5	23.28	21.72	10.71	7.60	7.84	10.35	...	10.86
NGC 5433	23.32	21.70	10.65	7.49	7.83	9.67	...	10.21
NGC 5426/7	23.09	21.81	10.55	7.66	7.94	10.42	...	10.83
ZW 247.020	23.79	21.51	11.03	7.32	7.57	10.14
NGC 5600	22.70	21.03	10.09	6.89	7.13	9.11	8.97	10.22	286	13.3
NGC 5653	23.36	21.63	10.74	7.49	7.72	9.23	9.76	10.49	240	9.5
NGC 5665	22.72	21.11	10.07	7.20	6.91	8.88	9.05	10.25	234	10.6
NGC 5676	22.97	21.55	10.42	7.42	7.68	9.77	9.96	10.42	577	2.9
NGC 5713	23.11	21.33	10.43	7.14	7.43	9.91	9.68	10.41	982	5.7
UGC 9618	24.09	22.51	11.45	8.35	8.65	>10.26	...	10.65
NGC 5792	22.78	21.37	10.15	7.16	7.50	10.01	...	10.32
ZW 049.057	23.75	21.70	11.02	7.48	7.76	...	9.55	9.71	...	29.5
NGC 5900	22.91	21.70	10.32	7.14	7.37	9.63	...	9.42
1 ZW 107	24.36	22.10	11.55	7.81	8.22	...	10.27	10.57	...	19.2
NGC 5929/30	23.05	21.15	10.34	6.92	7.24	9.34	10.19	9.42	575	8.3
IR 1525+36	24.46	22.20	11.61	7.80	8.34	10.48
NGC 5936	23.38	21.60	10.73	7.43	7.69	9.41	9.80	10.54	330	8.4
NGC 5937	23.45	21.49	10.83	7.33	7.61	9.21	...	10.39
NGC 5953/4	22.88	21.29	10.21	7.06	7.42	9.30	9.48	10.21	437	5.4
ARP 220	24.73	22.60	11.94	8.29	8.69	10.48	10.41	10.44	285	33.5
IR 1533-05	23.80	21.91	11.09	7.71	8.02	10.01
NGC 5962	22.78	21.31	10.19	7.15	7.43	9.48	9.46	10.34	418	5.3
NGC 5990	23.37	21.42	10.69	7.25	7.49	9.23	...	10.62
NGC 6052	23.40	21.53	10.69	7.32	7.64	9.88	...	10.53
MCG+01-42-088	23.85	21.90	11.14	7.71	8.00	9.48	...	10.46
NGC 6181	22.96	21.33	10.37	7.20	7.44	9.75	9.79	10.38	746	3.9
NGC 7448	22.84	21.19	10.22	7.02	7.29	9.75	9.06	10.39	640	14.4
NGC 7469 ^p	24.06	22.01	11.30	7.73	8.11	9.47	10.33	10.90	460	9.2
NGC 7479	23.18	21.50	10.48	7.25	7.62	9.94	10.06	10.64	1141	2.6
ZW 453.062	23.85	21.78	11.10	7.56	7.88	9.46	...	10.29
NGC 7541	23.40	21.70	10.76	7.52	7.80	10.19	9.95	10.44	726	6.5
ZW 475.056	24.02	21.90	11.25	7.66	7.99	9.74	10.03	10.44	348	16.7
NGC 7591	23.53	21.73	10.84	7.53	7.83	10.23	9.96	10.40	771	7.6
NGC 7592	23.88	21.96	11.12	7.69	8.09	10.07	10.32	10.69	677	6.3
NGC 7674	23.86	21.10	11.12	7.84	8.24	10.33	10.61	10.83	891	3.2
NGC 7678	23.17	21.59	10.54	7.41	7.71	9.82	9.52	10.66	389	10.5
NGC 7679	23.53	21.59	10.79	7.35	7.70	9.80	...	10.64
NGC 7714	23.15	20.97	10.37	6.68	7.06	9.79	9.33	10.25	1739	11.0
NGC 7771	23.81	22.04	11.14	7.86	8.15	9.95	10.18	10.58	332	9.3
MRK 331	23.97	21.81	11.18	7.53	7.90	9.96	10.37	10.07	964	6.5
UGC 12914/5	23.32	21.77	10.70	7.60	7.89	10.27	...	10.68

Notes to Table 4

(1) 60 μ m luminosity. (2) 850 μ m luminosity. (3) FIR luminosity calculated by integrating the measured SED from 40–1000 μ m. (4) Dust mass calculated using a single temperature, derived from fitting the 60,100 and 850 μ m fluxes. (5) Dust mass (M_d^{cold}) calculated using a two-component temperature fit to the data, assuming a cold $T_d = 20$ K and $\beta = 2$. (6) HI refs:- Bottinelli et al. (1990), Huchtmeier & Richter (1989), Theureau et al. (1998) (7) H₂ refs:- Young et al. (1995), Solomon et al. (1997), Sanders et al. (1991), Chini, Krügel & Lemke (1996), Maiolino et al. (1997), Casoli et al. (1996), Lavezzi & Dickey (1998), Sanders et al. (1986), Sanders & Mirabel (1985). (8) Blue luminosity calculated from B_T taken from the LEDA database and corrected for galactic extinction but not for internal extinction or inclination effects. (9) G_d is the gas-to-dust ratio calculated from HI + H₂ and the single temperature dust mass. (10) The FIR luminosity per unit gas mass (molecular); often used as a measure of the star formation efficiency of a galaxy. ^p NGC 7469 includes masses for IC 5283, except for HI which is for NGC 7469 only.

where D is defined in Eqn. 2 and C is a colour correction factor which depends on the ratio of S_{60}/S_{100} and the assumed value of the emissivity index. The correction factor, designed to account for emission outside the *IRAS* bands, varies between 1.3 and 2.4 and is explained in more detail by Helou et al. (1988). Having submillimetre fluxes, we can use our derived temperatures and β to integrate the total flux under the SED directly out to 1000 μ m, hopefully leading to more accurate values for L_{fir} since no general assumptions are being made. We integrate from 40 – 1000 μ m, since if we were integrating to shorter wavelengths we should really include the *IRAS* 12 and 25 μ m data points which would require a multi-component temperature model, beyond the scope of what we are doing here. However, for our objects the ratio of S_{60}/S_{25} is greater than 2.4, meaning that the contribution to the integral at $\lambda < 40\mu$ m is not very significant (if we integrate our SED with only the three data points out to 1 μ m we find increases in L_{fir} of only a few per cent). Our values for L_{fir} are similar to those calculated using the standard *IRAS* formulation described above, although slightly lower (~ 10 per cent) than if the appropriate value of C were chosen for an emissivity index of one. This is probably because calculating a temperature from the 60/100 flux ratio tends to overestimate the temperature and therefore the correction factor required. It must be noted that the true SED of these galaxies may not be well represented by a single temperature model and the values of L_{fir} would change accordingly. Our integrated values for L_{fir} are listed in Table 4.

4 LUMINOSITY AND DUST MASS FUNCTIONS

The luminosity function (LF) is given by

$$\Phi(L)\Delta L = \sum_i \frac{1}{V_i} \quad (5)$$

where $\Phi(L)\Delta L$ is the number density of sources (Mpc^{-3}) in the luminosity range L to $L + \Delta L$, the sum is over all

Table 6. Conversion factors used for CO data

Telescope	Beam size "	Scale	Conversion (Jy K ⁻¹)	Refs
FCRAO	45	T_A^*	42	a
		T_R^*	31.5	d, h, i
SEST	45	T_{mb}	19	b
IRAM	22	T_{mb}	4.5	c
NRAO	55	T_R^*	35	d, e, i
		T_{mb}	30	f, g

Reference Key :- (a) Young et al. (1995), (b) Chini et al. (1996), (c) Solomon et al. (1997), (d) Sanders et al. (1991), (e) Maiolino et al. (1997), (f) Casoli et al. (1996), (g) Lavezzi & Dickey (1998), (h) Sanders et al. (1986), (i) Sanders & Mirabel (1985)

the sources in the sample in this luminosity range, and V_i is the accessible volume of the i th source in the original sample (Avni & Bahcall 1980). For this sample, the accessible volume is the maximum volume in which the object could be seen and still be in the *IRAS* Bright Galaxy Sample and so to calculate this, the 60 μ m luminosity of each galaxy is used. In Equation 5, however, the luminosity is the luminosity at 850 μ m, the wavelength of our survey. The volume from $cz = 0$ to $cz = 1900 \text{ km s}^{-1}$ is not included in the calculation of V_i as galaxies with velocities less than this were excluded from our sample. $\Phi(L)$ has been normalised to dex^{-1} by dividing by ΔL . The dust mass function is estimated in the same way as the luminosity function but substituting dust mass for luminosity in Eqn. 5. This was done for both values of the dust mass; using a single temperature, and assuming a colder component at $T_d = 20$ K. The luminosity function at 850 μ m and both of the dust mass functions are shown in Fig. 5, and tabular forms for the functions are given in Table 7.

The BGS contains many close pairs which are resolved at 850 μ m but not at the *IRAS* wavelengths. A few do have HIRES fluxes (Surace et al. 1993) and, when the resolved 60 μ m flux is still above the 5.24 Jy limit of the sample, can be treated as separate objects for the purposes of calculating the luminosity and dust mass functions. The effect on the luminosity function of separating sources in this way would be to steepen it, as one luminous source with a large accessible volume becomes two less luminous sources with smaller volumes. We attempted to quantify this in the following way. For galaxies without HIRES fluxes, we estimated 60 μ m fluxes for the individual galaxies in each pair using the FIR-radio correlation (Helou et al. 1985). We removed any galaxy whose flux fell below the flux limit of the sample and re-calculated the luminosity function. Figure 6 shows this luminosity function compared with our original one (calculated using the sum of the 850 μ m emission from a pair of galaxies unresolved at 60 μ m). There is only a significant difference in the highest luminosity bin, which suffers from noise anyway due to the small number of objects. In future, we will refer only to the luminosity function constructed using the combined pair fluxes (Fig. 5a), since this can be most readily compared with the 60 μ m LF.

The luminosity function estimator (Eqn. 5) is unbiased providing there is no population of submillimetre emitting

Table 5. Luminosities and masses for pairs resolved by SCUBA

Name	$\log L_{60}$ (W Hz ⁻¹ sr ⁻¹)	$\log L_{850}$ (W Hz ⁻¹ sr ⁻¹)	$\log L_{\text{fir}}$ (L _⊙)	$\log M_{\text{d}}$ (M _⊙)	$\log M_{\text{d}}^{\text{cold}}$ (M _⊙)	$\log M_{\text{HI}}$ (M _⊙)	$\log M_{\text{H}_2}$ (M _⊙)	$\log L_{\text{B}}$ (L _⊙)	G_{d}
IC 563	23.28	21.78	10.65	7.59	7.92	10.10	...	10.09	...
IC 564	23.21	21.86	10.66	7.73	8.00	10.35	...
NGC 3994	23.04	21.22	10.29	7.07	7.33	9.75	...	9.86	...
NGC 3995	23.11	21.34	10.16	7.14	7.47	10.09	...	10.33	...
NGC 5257	...	21.92	...	7.69	...	10.27	...	10.69	...
NGC 5258	...	22.09	...	7.85	...	10.23	...	10.71	...
NGC 5394	...	21.14	...	7.02	...	9.95	...	10.06	...
NGC 5395	...	21.59	...	7.47	...	10.13	...	10.49	...
NGC 5426	22.56	21.51	10.06	7.36	7.64	10.16	...	10.22	...
NGC 5427	22.95	21.51	10.38	7.36	7.63	10.08	...	10.62	...
UGC 9618 (N)	...	22.32	...	8.17	...	>10.26	...	10.59	...
UGC 9618 (S)	...	22.07	...	7.91	10.28	...
NGC 5929	...	20.41	...	6.19	...	8.93	9.06	9.61	1291
NGC 5930	...	21.05	...	6.83	...	9.08	9.14	9.85	373
NGC 5953	...	21.07	...	6.84	...	9.06	9.27	9.70	435
NGC 5954	...	20.90	...	6.67	...	8.93	9.05	9.54	423
NGC 7469	...	21.87	...	7.52	...	9.48	10.11	10.62	480
IC 5283	...	21.44	...	7.27	9.94	9.78	...
UGC 12914	...	21.61	...	7.44	...	9.99	...	10.49	...
UGC 12915	...	21.69	...	7.52	...	9.95	...	10.13	...

Columns have the same meanings as in Table 4

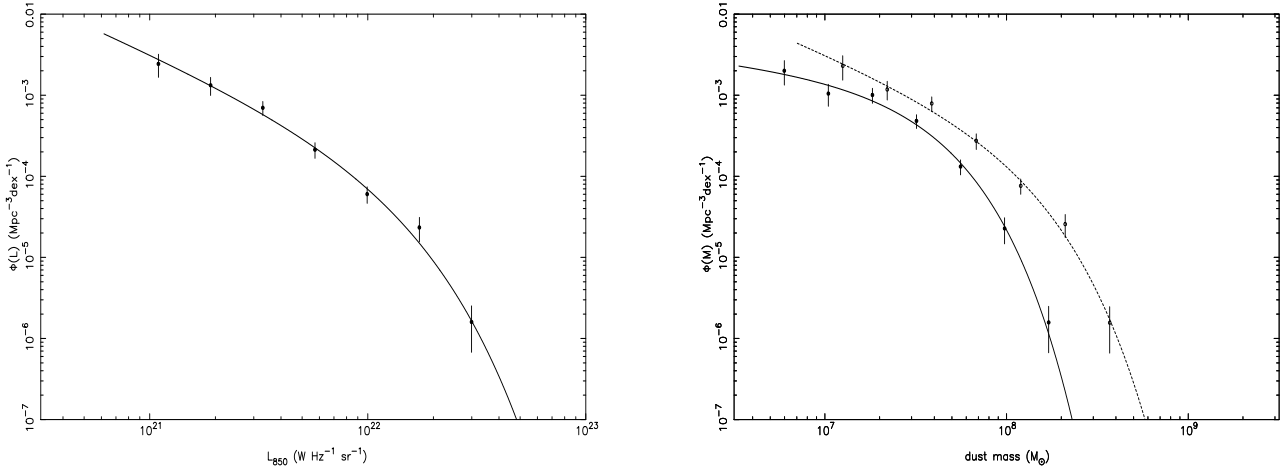


Figure 5. a) Luminosity function at 850 μm shown with best-fitting Schechter function, $\alpha = -2.18$, $L_* = 8.3 \times 10^{21} \text{ W Hz}^{-1} \text{ sr}^{-1}$. b) Dust mass function. Solid line:– dust masses calculated from the submillimetre fluxes using the best-fitting β and T_{d} . Schechter parameters shown are $\alpha = -1.23$, $M_* = 2.5 \times 10^7 M_{\odot}$. Dashed line:– ‘cold dust mass’ function using $T_{\text{cold}} = 20 \text{ K}$ and $\beta = 2$. Schechter parameters are $\alpha = -1.91$ and $M_*^{\text{cold}} = 8.5 \times 10^7 M_{\odot}$.

galaxies which have a high space density, yet are completely absent from the original *IRAS* sample. The only conceivable type of galaxy to which this could apply would be a hypothetical ‘cold’ population with $T_{\text{d}} < 25 \text{ K}$. To investigate this possibility, let us assume that there are two populations of galaxies with equal space densities and 850 μm luminosities, one with dust temperatures at 20 K and the other at 35 K. The relative numbers in an 850 μm flux-limited survey would be given by

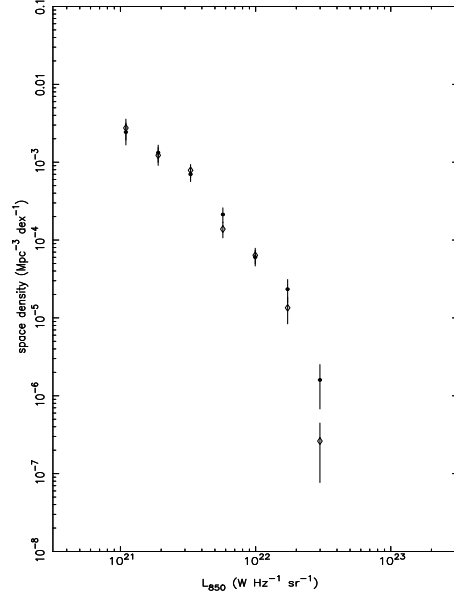
$$\frac{N_A}{N_B} = \frac{\Phi_A}{\Phi_B} \times \frac{V_A}{V_B} \approx \frac{\Phi_A}{\Phi_B} \frac{(L_{850,A})^{3/2}}{(L_{850,B})^{3/2}}$$

where A and B refer to the two populations, Φ is the space density, V is the ‘accessible volume’ in which one of the galaxies would have been detected by the survey, and L_{850} is the luminosity at 850 μm . Given the assumptions we have made, $N_A/N_B = 1$ and therefore equal numbers of the two populations should be found by the survey.

Table 7. Local luminosity function at 850 μ m

$\log L_{850}$ (W Hz ⁻¹ sr ⁻¹)	$\phi(L)$ (Mpc ⁻³ dex ⁻¹)	σ_ϕ (Mpc ⁻³ dex ⁻¹)	
21.04	2.43e-3	7.69e-4	
21.28	1.33e-3	3.32e-4	
21.52	7.00e-4	1.37e-4	
21.76	2.13e-4	4.65e-5	
22.00	6.02e-5	1.38e-5	
22.24	2.34e-5	7.8e-6	
22.48	1.60e-6	9.2e-7	
α	L_* (W Hz ⁻¹ sr ⁻¹)	ϕ_* (Mpc ⁻³ dex ⁻¹)	χ^2_ν
$-2.18^{+0.22}_{-0.24}$	$8.3^{+2.5}_{-2.0} \times 10^{21}$	$2.9^{+4.1}_{-1.5} \times 10^{-4}$	0.68
Single temperature dust mass function			
$\log M_d$ (M _⊙)	$\phi(M)$ (Mpc ⁻³ dex ⁻¹)	σ_ϕ (Mpc ⁻³ dex ⁻¹)	
6.78	2.00e-3	6.68e-4	
7.02	1.05e-3	3.16e-4	
7.26	1.01e-3	2.10e-4	
7.50	4.82e-4	9.28e-5	
7.75	1.32e-4	2.75e-5	
7.99	2.27e-5	8.0e-6	
8.23	1.58e-6	9.1e-7	
α	M_* (M _⊙)	ϕ_* (Mpc ⁻³ dex ⁻¹)	χ^2_ν
$-1.23^{+0.44}_{-0.59}$	$2.50^{+0.95}_{-0.82} \times 10^7$	$1.64^{+0.69}_{-0.48} \times 10^{-3}$	0.56
Cold component dust mass function			
$\log M_d^{cold}$	$\phi(M)$	σ_ϕ	
7.10	2.30e-3	7.67e-4	
7.34	1.18e-3	3.04e-4	
7.59	7.91e-4	1.61e-4	
7.83	2.74e-4	5.99e-5	
8.08	7.63e-5	1.63e-5	
8.32	2.57e-5	8.13e-6	
8.57	1.56e-6	9.02e-7	
α	M_*^{cold}	ϕ_*	χ^2_ν
$-1.91^{+0.21}_{-0.24}$	$8.5^{+2.2}_{-1.9} \times 10^7$	$4.9^{+3.3}_{-2.2} \times 10^{-4}$	0.62

Now let us consider the relative numbers that would be found by a 60 μ m flux-limited survey (the BGS). Replacing the 850 μ m luminosity in the above equation with 60 μ m luminosity, we now predict that the ratio N_{35K}/N_{20K} will be ~ 724 . Clearly, in a sample of ~ 100 *IRAS* galaxies, finding a member of this hypothetical cold population would be unlikely and so our attempt to construct the 850 μ m LF from our sample would be an underestimate. Making a similar calculation for galaxies at $T_d = 25$ K and 35 K we now ex-

**Figure 6.** Luminosity function at 850 μ m for combined pair fluxes (Table 1) – solid symbols, compared to the luminosity function when the fluxes for the resolved pairs are separated (Table 2) – open symbols.

pect to find ~ 32 times as many warm galaxies as cold ones, so in our sample we would expect to see around 3 objects at $T_d = 25$ K. There are actually two galaxies with $T_d \sim 25$ K in our sample, which is consistent with the idea that we could be missing a significant cold population.

Is there truly a possibility that there is a missing population of galaxies? An important point to realise is that our dust temperatures are merely those corresponding to a best-fitting single-component model and are not *actual* dust temperatures. One way to assess the possibility that we are missing galaxies is to carry out precisely the same fitting procedure for optically-selected galaxies. For example, NGC 891 has been studied at many submillimetre wavelengths (Alton et al. 1998b), but if we throw away all the measurements except those at 60, 100 and 850 μ m, and carry out our fitting procedure, we obtain $T_d = 34$ K and $\beta = 0.7$. While this temperature is similar to the average temperature for our sample, indicating that there is a warm component in NGC 891, the value of 0.7 for β is significantly lower than for most of our galaxies suggesting a large amount of colder dust, and when the full submillimetre data-set was used the bulk of the dust in NGC 891 was found to be at 15 K. Consider now our own Galaxy : if the *IRAS* FIR and ARGO submillimetre data (Sodroski et al. 1989; Masi et al. 1995) for the Milky Way is combined and fitted in our usual way we find a temperature of 28 K with a β of 0.7, so again the SED of the Milky Way would not necessarily have excluded it from our sample. The question of whether we are missing cold galaxies remains open (primarily how many cold galaxies there are to miss). To address this properly, and to constrain the luminosity function better at low luminosities we will need to complete the survey of an optically-selected sample, which will not be biased by temperature selection as is the BGS.

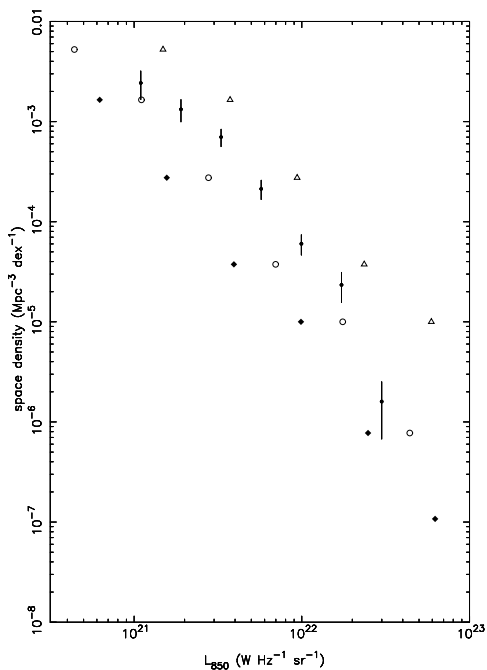


Figure 7. The measured 850 μ m luminosity function (solid symbols with error bars) along with extrapolations of the 60 μ m LF from Soifer et al. (1987), using the following fixed parameters: $\beta = 2$, $T_d = 24$ K – open triangles; $\beta = 1.5$, $T_d = 38$ K – solid diamonds; $\beta = 1$, $T_d = 45$ K – open circles.

The 60 μ m luminosity function of the BGS from Soifer et al. (1987), can be compared to the 850 μ m LF by making an extrapolation based on an assumption about a galaxy’s SED from the far-infrared to the submillimetre. In fact, all of the 60 μ m LFs using *IRAS* data are consistent with each other (with the exception the one from Saunders et al. (1990), see Lawrence et al. 1999) and so it does not really matter which one we use. We have used the Soifer et al. one as it represents the same sample of galaxies which we observed. In the past this extrapolation has been done by assuming a single temperature and β for all galaxies, which for 60 and 850 μ m gives the following

$$L_{850} = L_{60} \times \left(\frac{\nu_{850}}{\nu_{60}} \right)^{3+\beta} \times \left(\frac{e^{240.2/T_d} - 1}{e^{16.8/T_d} - 1} \right) \quad (6)$$

Extrapolations of the 60 μ m LF using a range of plausible values of β and T_d are shown over the measured 850 μ m LF in Fig 7. As one would expect, an 850 μ m luminosity function obtained by extrapolating in wavelength from a 60 μ m LF is highly dependent on the values assumed for T_d and β . In practice, luminosity functions obtained in this way have had much lower amplitudes than the one we actually measure, essentially because dust temperatures deduced from *IRAS* data alone are always higher than the temperatures we estimate here. This can have significant consequences when trying to model the evolution required to fit the observed submillimetre number counts from deep surveys and the submillimetre background and the implications will be discussed in a future paper (Eales et al. in prep). The other difference in the luminosity functions is the slope: the luminosity function we measure is steeper than the ones extrapolated from the 60 μ m LF. The difference in slope between the

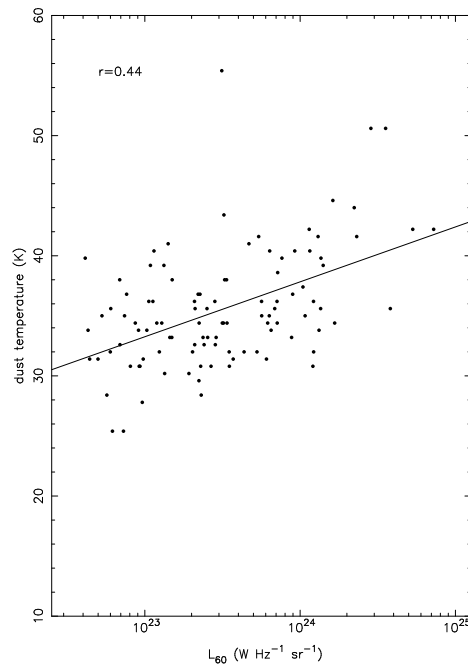


Figure 8. Dust temperature T_d versus 60 μ m luminosity, showing that the most luminous galaxies have the hottest temperatures, the abrupt cutoff at the low luminosity end is due to the lower velocity limit in the selection of the sample at 60 μ m.

two LFs is due to the correlation of dust temperature with 60 μ m luminosity (Fig. 8). As the temperature changes with 60 μ m luminosity, extrapolating every L_{60} to 850 μ m with an average T_d will underestimate the 850 μ m luminosity at lower L_{60} and overestimate it at high L_{60} . Using the fitted dependences of L_{60} on T_d and also β on T_d (see Table 8) we again extrapolate the 60 μ m LF and this time the agreement with the 850 μ m LF is much better (Fig. 9).

The 850 μ m luminosity and dust mass functions are well fitted by Schechter functions of the form (Press & Schechter 1974; Schechter 1975)

$$\Phi(L)dL = \phi(L) \left(\frac{L}{L_*} \right)^\alpha e^{-(L/L_*)} dL/L_*$$

The best fitting parameters for the 850 μ m LF and the dust mass functions along with the reduced chi-squared values (χ_ν^2) for the fits, are given in Table 7. The χ^2 contours showing the joint confidence intervals on α and L_* for all the functions are shown in Figs. 10(a-c).

There are several points to note here. Firstly, the 60 μ m LF cannot be fitted by a simple Schechter function (Lawrence et al. 1986; Rieke & Lebofsky 1986) as the high luminosity end does not fall off steeply enough. The fact that the 850 μ m LF and the dust mass function can, suggests that the Schechter function is surprisingly universal and that in the case of the 60 μ m LF, the Schechter function exponential fall-off is concealed by the sensitivity of the 60 μ m emission to dust temperature. Secondly, the slope of the 850 μ m LF is steeper than -2 ($\alpha = -2.18$) at lower submillimetre luminosities. This is significant because if this slope continued to zero luminosity, the submillimetre sky would be infinitely bright (a submillimetre Olbers Paradox). Of course, this means that the slope must flatten out at lower luminosities not yet probed by our survey. The shape of the

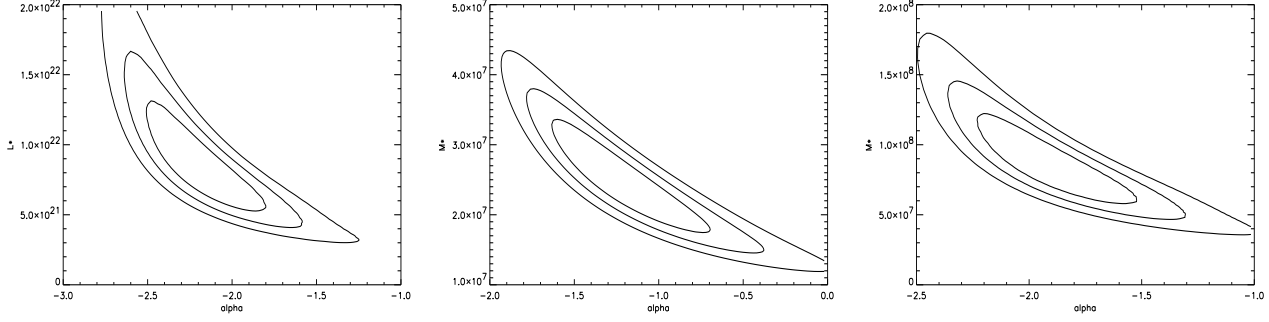


Figure 10. a) Joint confidence χ^2 contours for the $850\mu\text{m}$ LF parameters α and L_* . Contours are at the 68, 90 and 95% confidence level, d.o.f = 2. b) Joint confidence contours for the single temperature dust mass function parameters α and M_* . Same contour levels as a). c) Joint confidence contours for the ‘cold’ dust mass function, same parameters and levels as b).

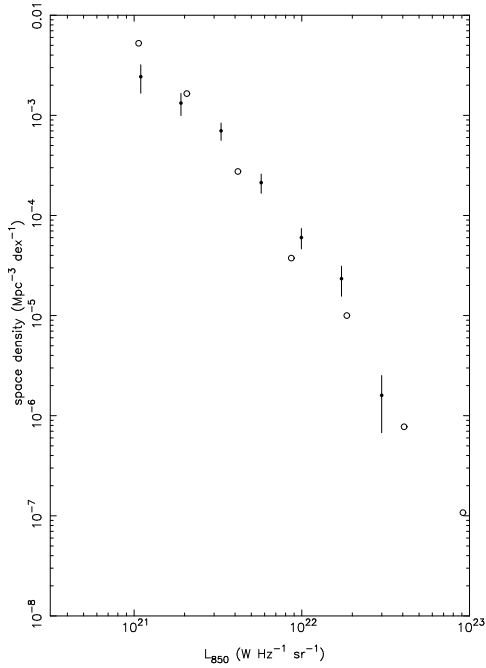


Figure 9. $850\mu\text{m}$ LF (solid symbols) along with the extrapolation of the Soifer et al. (1987) $60\mu\text{m}$ LF using variable β and T_d given by the relationships in Table 8. This produces a better match to the measured $850\mu\text{m}$ LF than extrapolations made using single values for T_d and β (see Fig. 7).

dust mass function is strongly affected by the temperature distribution assumed, i.e. all of the dust at a single temperature, or most of the dust at some colder temperature with a small warmer component being responsible for the $60\mu\text{m}$ flux. The shape of the ‘cold dust mass’ function bears more resemblance to the $850\mu\text{m}$ LF simply because of our assumption of a common universal temperature for the cold component. We do believe however, that the true distribution of the dust masses lies somewhere between the two; the temperature of a cold component may not be the same in all galaxies but will probably vary less than the temperature of the warm components and this degree of variation along with the relative amounts of cold and warm dust will

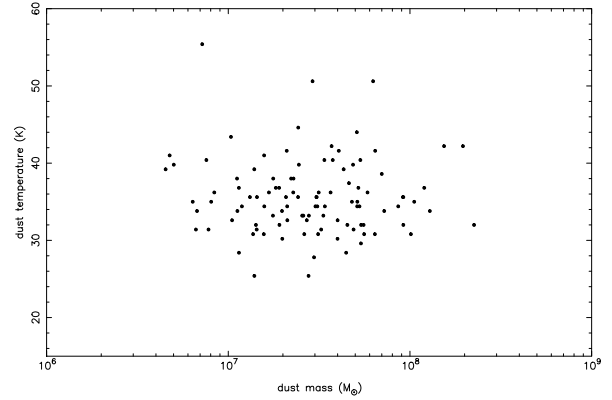


Figure 11. Plotting dust temperature versus dust mass shows no correlation. This means that $L_{60}-T_d$ relationship (Fig. 8) is not a function of dust mass.

determine how similar the dust mass function is in shape to the $850\mu\text{m}$ LF.

5 DISCUSSION

5.1 Correlations

5.1.1 Dust temperature

Luminosity is often strongly correlated with mass in astrophysical situations, and so at first sight the $L_{60} - T_d$ correlation (Fig. 8) suggests that the more luminous systems are hotter. We can test this by plotting dust temperature versus dust mass and blue luminosity, often used as a measure of the mass of a galaxy. In the first case (Fig. 11) there is no significant correlation (see Table 8 for coefficients), so there is no tendency for galaxies with lots of dust to be hotter, and in the second case (Fig. 12) there is an inverse correlation. The $L_{60} - T_d$ correlation is therefore most naturally explained by the sensitivity of the $60\mu\text{m}$ flux to the dust temperature. If, for whatever reason (and not because of its mass) the dust is hotter, this will greatly increase the $60\mu\text{m}$ luminosity. What is rather more interesting (and perhaps surprising) is the anti-correlation of the corrected L_B ver-

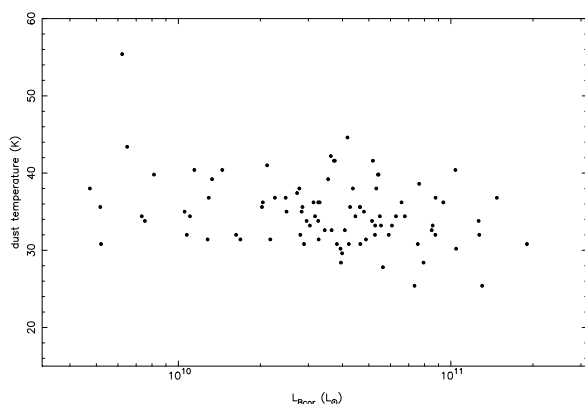


Figure 12. A plot of dust temperature against blue luminosity shows an anti-correlation ($r = 0.2$). This is quite surprising as initially it was thought that the $L_{60}-T_d$ correlation was due to galaxy mass (i.e. larger galaxies have more $60\mu\text{m}$ luminosity and therefore higher dust temperatures).

sus T_d (Fig. 12). The significance is at the 98 per cent level, making it the least secure of the correlations we present here and the probable link is with the star formation efficiency rather than dust temperature itself. Using $L_{\text{fir}}/M_{\text{H}_2}$ as a measure of star formation efficiency, Young (1999) has recently found that the star formation efficiency of galaxies in many different types of environment decreases as galaxy size increases (as measured by the optical linear diameter D_{25}). If we now plot $L_{\text{fir}}/M_{\text{H}_2}$ against L_B for our galaxies a much better correlation is seen than with T_d , indicating that this is where the true dependence lies (see Fig. 13 and Table 8). The explanation Young gives for this relationship is that larger galaxies have flatter rotation curves over more of their disks and so experience more shear. She suggests that the effect of this would be to reduce the ability of molecular clouds to form stars by increasing the turbulence within them, and to dampen the effects of star-formation triggers.

5.1.2 Gas and dust masses

We compared the dust masses, derived from the submillimetre fluxes using a single temperature, to the H_2 , HI and $\text{H}_2 + \text{HI}$ masses as shown in Figure 14a-c. The strongest correlation is with the molecular gas which suggests that the dust is primarily found in molecular clouds. The larger scatter on the HI plots may be because we are using global HI values which may include gas at very large radii where there would be much less dust than in the inner disk. Devereux & Young (1990) found that if they only used the HI in the inner disk, in addition to the molecular gas, then the correlation between gas and dust was improved. We cannot, however, investigate the spatial connection between dust and atomic gas in the region they both occupy as we do not yet have HI maps. We repeated the process using the ‘cold dust masses’ but found no differences in the correlations or slopes of the plots and so have not included these.

We would like to try to address the reasons behind the tightness of the relationship between dust and molecular gas. The scatter in this plot (Fig. 14a) is very small, the r.m.s dispersion about the line of best fit is only ~ 60 per cent. Some of

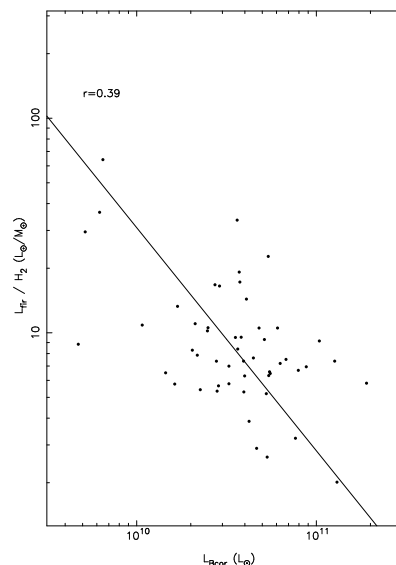


Figure 13. A stronger anti-correlation is seen when the dust temperature from Fig. 12 is replaced by a measure of the star formation efficiency ($L_{\text{fir}}/M_{\text{H}_2}$). This is the explanation for the weak dependence on dust temperature in Fig. 12, as L_{fir} is a function of T_d . This figure suggests that smaller galaxies have larger star formation efficiencies, a trend first noticed by Young (1999).

this is due to observational errors; if we assume 30 per cent errors in the fluxes and subtract this in quadrature from the overall value then we are left with 52 per cent as the intrinsic scatter. There are some observational-type errors which are hard to account for, such as aperture corrections and the probability that our assumption of a single dust temperature is wrong, but the small scatter does suggest that any aperture effects must be similar for all the galaxies and that if our assumption about temperature is wrong then it must be wrong in the same way for all of the galaxies. This is borne out by the similarity of the relationship when the ‘cold dust masses’ are used.

In order to determine the physical meaning of the 50 per cent scatter we will review the current views on the formation of dust and CO and the expected dependences on metallicity. There are no firm conclusions about how dust grains form. Suggested sites of formation range from post-AGB stars to supernova remnants (Whittet 1992). The grains are thought to grow in the darkest molecular clouds by accretion of icy mantles and are probably destroyed by sputtering in the diffuse ISM, after the dispersion of the molecular cloud by supernova shocks and HII regions. Despite the complications in determining how and where the various stages of dust evolution occur, there is some evidence that the fraction of metals bound up in dust grains is a constant, both from observations of nearby galaxies (Issa et al. 1990) and from observations in our own Galaxy, where the carbon and oxygen abundances (the main constituents of dust) are constant over a wide range ISM densities (Cardelli et al. 1996; Meyer et al. 1998). This suggests that $M_d \propto Z M_g$ where M_g is the total mass of gas and Z is the metallicity.

The formation of CO is better understood than that of dust and is believed to occur through a network of gas-phase

Table 8. Parameters for fits and correlations

y	x	Number	r_s	significance	linear fit: $y = mx + c$	
					m	c
T_d	$\log L_{60}$	104	0.44	$2.5e-6$	4.57 ± 0.82	-71.9 ± 19.4
T_d	$\log M_d$	104	-0.02	0.8		
T_d	$\log L_B^c$	91	-0.25	0.02		
β	T_d	104	0.44	$3.7e-6$	-0.0184 ± 0.004	1.95 ± 0.13
$\log M_d$	$\log M_{H_2}$	59	0.89	$6.2e-21$	0.82 ± 0.04	-0.67 ± 0.38
$\log M_d$	$\log M_{HI}$	84	0.64	$3.6e-11$	0.94 ± 0.09	-1.81 ± 0.68
$\log M_d$	$\log M_{H_2+HI}$	47	0.86	$7e-15$	0.96 ± 0.06	-2.32 ± 0.53
$\log L_{fIR}$	$\log M_{H_2}$	59	0.81	$1.4e-14$	1.14 ± 0.09	-0.39 ± 0.78
$\log L_{fIR}/M_{H_2}$	$\log L_B^c$	52	-0.39	$3.9e-4$	-1.04 ± 0.20	11.89 ± 0.59

NOTES – *Column(4)*– Spearman rank correlation coefficient. *Column(5)*– probability that x and y are unrelated. c :- luminosity corrected for galactic and internal extinction and for inclination effects.

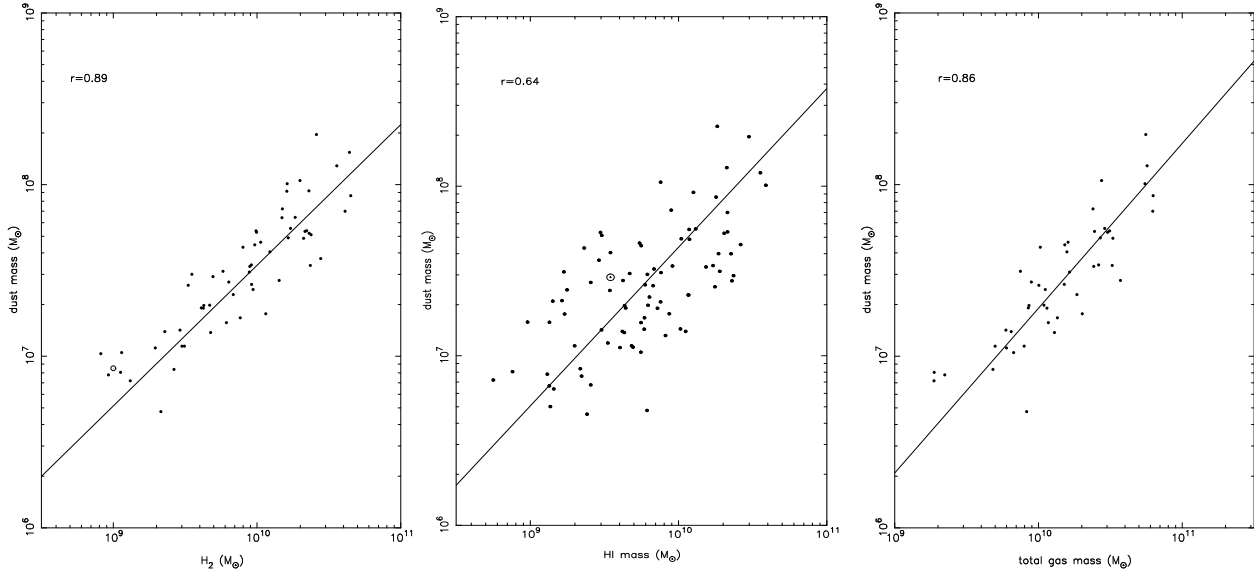


Figure 14. a) Dust mass versus H_2 mass, a solar symbol indicates the Milky Way values (Sodroski et al. 1994). The line is the best least squares fit (see Table 8 for fit parameters). b) Dust mass versus HI mass, the line indicates the best least squares fit to the data. There is much more dispersion than for Fig. 14a. c) Dust mass versus $H_2 + HI$ mass.

reactions in the giant molecular clouds (GMCs). CO will form readily, the rate increasing with density, but is easily destroyed by UV radiation. In order to remain intact, the CO needs to be shielded by dust grains and/or large column densities of H_2 . Assuming that the dominant mass in the GMCs is in the form of H_2 , then since CO forms from the C and O available in the gas-phase, (and O is always more abundant than C in the ISM), a metallicity dependence is suggested where $L_{CO} \propto ZM_{H_2}$. However, since most of the shielding required to form the CO is produced by dust rather than H_2 , the true metallicity dependence may be even higher than this. When there is insufficient dust in a molecular cloud to provide adequate shielding from the UV radiation field, the volume of the cloud occupied by CO may not be as large as that occupied by H_2 , because H_2 is more efficient at self-shielding. This is the likely case in

low metallicity systems such as the LMC or where the volume and/or column densities are low. The possibilities that CO and H_2 may not always be co-extensive, and that there may be a dependence of CO luminosity on metallicity, can lead to problems with the application of the X factor to CO observations in order to determine the mass of H_2 . For systems with significantly lower densities and/or metallicities a larger conversion may be needed relative to galaxies such as the Milky Way. Observations do indicate a dependence of X on metallicity for low metallicity systems (Wilson 1995) with $X/X_G = (Z/Z_\odot)^{-0.7}$ for systems with less than solar metallicity and staying roughly constant for higher than solar metallicities (Frayer & Brown 1997). This observed dependence is less steep than one would have imagined from the above simplistic arguments. It could be argued that for metallicities above some critical value, where there is suffi-

cient shielding, the X factor may show less dependence on metallicity, as the abundance of CO relative to H_2 depends on the availability of C and O and not on dust any longer. While the formation of CO should still be greater for higher metallicities, H_2 formation is also dependent on dust grains as catalysts so it is possible that this could cause the X factor to saturate: more metals lead to more CO, but they also lead to more dust and thus more H_2 formed from atomic hydrogen, producing the observation that the X factor is constant with metallicity above a threshold value. Theory does predict significant depletion of CO onto dust grains (forming mantles) for favourable conditions in the cloud which would make X smaller with increasing metallicity, possibly offsetting any trend for an increase but in the Milky Way this depletion is only observed to be 5 to 40 per cent (Whittet 1992), much less than predicted, indicating that there is still much which is not understood about the interaction of dust and molecules in the GMCs.

We do not have metallicity measurements for our galaxies, but the range of metallicities of spiral galaxies of similar absolute magnitudes is 2–3 (Henry & Worthey 1999). Thus the small scatter in the H_2 –dust mass diagram strongly suggests that the metallicity dependence of dust mass and of the CO X factor is very similar. An additional test of this will be extending our study to galaxies likely to have a larger range of metallicity.

5.1.3 Star formation efficiency

The ratio of L_{fir}/M_{H_2} is often used as a measure of the star formation efficiency of a galaxy since L_{fir} is believed to trace the star formation rate and so this ratio gives the star formation rate per unit gas mass. Figure 15 shows the strong correlation between molecular gas and L_{fir} and gives some idea of the range of L_{fir}/M_{H_2} values for these galaxies. The $L/M = 4$ line represents ‘normal’ galaxies such as the Milky Way (Scoville & Good 1989) and most of the galaxies in our sample show elevated star formation efficiencies relative to the Milky Way. Many of the galaxies lying above the general trend ($SFE \geq 20$) are often interacting or have suspected active nuclei (e.g. IR 0857+39 with $SFE \sim 100$). Values of L_{fir}/M_{H_2} are given in Table 4.

5.2 Gas to dust ratios

The average gas-to-dust ratios (using the single temperature dust masses) for the three components are $M_{H_2}/M_d = 293 \pm 19$, $M_{HI}/M_d = 304 \pm 24$ and $M_{H_2+HI}/M_d = 581 \pm 43$, where the \pm indicates the error in the mean. In future, we will refer to M_{H_2+HI}/M_d as the gas-to-dust ratio G_d and the values are listed in Table 4. In order to compare our G_d with the Galactic value, we must be careful that we account for the differences in $\kappa_d(\nu)$ and X used by others and ourselves. The gas-to-dust ratio for the Milky Way was measured by Sodroski et al. (1994), using *COBE* data at 140 and 240 μm , therefore in order to compare our measurement with theirs we must also scale the $\kappa_d(240)$ value of the opacity coefficient they used to 850 μm , using an assumed value for β . Sodroski et al. use a $\kappa_d(240) = 0.72 \text{ m}^2 \text{ kg}^{-1}$; taking this to 850 μm gives $\kappa_d(850) = 0.2 - 0.057 \text{ m}^2 \text{ kg}^{-1}$ for $\beta = 1 - 2$. Comparing this to our value of $0.077 \text{ m}^2 \text{ kg}^{-1}$ and accounting for the

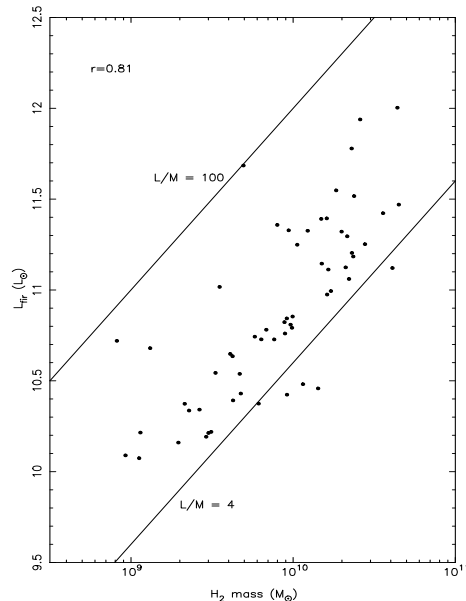


Figure 15. FIR luminosity versus H_2 mass. The quantity L_{fir}/M_{H_2} is taken as a measure of the star formation efficiency of the galaxy. The galaxies lying above the trend are mostly interacting or with suspected active nuclei. Our Galaxy is believed to lie on the $L/M \sim 4$ line and so most of the galaxies in our sample would appear to be more efficient than the Milky Way.

differences in X factors (theirs being 0.71 times ours) gives a range of Galactic G_d values of 85–302 for a β of $1 \rightarrow 2$. The middle of the range at $\beta = 1.5$ is $G_d = 160$ and this is the nominal value we will make comparisons with. It can now be seen that our average gas-to-dust ratio of 581 is more than a factor of three larger than the Galactic value of 160 (at the least a factor of 2 larger if $\beta = 2$). Of course, the measurement made by Sodroski et al. is a very difficult one to make, but it is supported by arguments based on element abundances and depletions which predict a ratio of ~ 130 (Eales et al. in prep). The Galaxy has a FIR luminosity of $1.1 \times 10^{10} L_\odot$ and a dust mass of $\sim 2.9 \times 10^7 M_\odot$ (Sodroski et al. 1994) which assumes the same value for $\kappa_d(\nu)$ that gives a $G_d = 160$. This places the Galaxy at the bottom end of the range of luminosities and dust masses found in this IR bright sample. Previous determinations of the gas-to-dust ratios in IR luminous objects using *IRAS* data have always been high ~ 1000 (Young et al. 1989; Devereux & Young 1990; Sanders et al. 1991) which has been attributed to the lack of sensitivity of *IRAS* to cold dust. It would seem that our submillimetre observations have reduced this tendency, giving a lower gas-to-dust value, but when the gas-to-dust ratios are re-calculated using the ‘cold dust masses’ we find a further reduction to $M_{H_2}/M_d^{\text{cold}} = 143 \pm 9$, $M_{HI}/M_d^{\text{cold}} = 158 \pm 14$ and $M_{H_2+HI}/M_d^{\text{cold}} = 293 \pm 24$. This is now just within the range of values we calculated for the Galaxy, and in good agreement if the $\beta = 2$ case is taken. We perform the calculations with the ‘cold masses’ simply to illustrate the effect of overlooking this component. A slightly colder temperature (say 15–18 K) would increase the dust masses by a larger amount, further reducing the observed gas-to-dust ratios and so giving better agreement with the Galactic values.

The gas-to-dust ratios calculated using the single temper-

ature dust masses vary from 1700 to 200, the large range being mostly due to the variations in $M_{\text{HI}}/M_{\text{d}}$ as discussed in Section 5.1.2. Some of the larger values of $M_{\text{H}_2}/M_{\text{d}}$ could be due to the large angular sizes of some of the nearer galaxies, meaning that our dust masses are underestimated when compared to the CO fluxes produced from multi-positional single dish measurements (this particularly applies to NGC 772 and NGC 7479); however this is not always the case as there are some galaxies of small angular size which have high $M_{\text{H}_2}/M_{\text{d}}$ ratios but more normal $M_{\text{HI}}/M_{\text{d}}$, (e.g. IR 0335+15, UGC 4881 and Mkn 331). These galaxies are interacting or have Seyfert nuclei and typically have high dust temperatures, which may suggest that the lack of apparent dust mass is simply due to using a high temperature when calculating M_{d} and not accounting for any colder dust. High temperatures cannot be the sole explanation, however, as other galaxies with high T_{d} and signs of interaction/activity have rather low values of $M_{\text{H}_2}/M_{\text{d}}$ (e.g. Arp 220). It could be that an enhanced $M_{\text{H}_2}/M_{\text{d}}$ is a stage that some merging/starburst galaxies pass through, either by an enhancement of CO relative to dust, or a decrease in dust emission. A change in the X factor, causing the H_2 to be overestimated could also be responsible (this has been suggested for many extreme active/starburst nuclei (Solomon et al. 1997)). It is also possible that CO which was depleted from the gas phase onto grain mantles in dark clouds could, at a certain stage in the starburst evolution, become vaporized back into the gas phase, giving a higher CO flux while keeping the atomic, dust and H_2 content the same. One particular case which deserves a mention here is NGC 7714 which has $M_{\text{HI}}/M_{\text{d}} \sim 1300$, causing its abnormally high gas-to-dust (G_{d}) value of 1700 (see column 9 of Table 4). NGC 7714 is interacting with NGC 7715 although they are widely spaced enough (1.9 arcmin) that only NGC 7714 was observed with SCUBA and the *IRAS* flux is due entirely to NGC 7714 (Surace et al. 1993). The HI maps of Smith et al. (1997) show rings and bridges of gas connecting the two galaxies, so it is probable that some of the HI listed for NGC 7714 in the single dish measurement (Table 4) is really associated with the whole region and cannot be compared with what we observed. The amount of HI contained in the 50×50 arcsec region centred on NGC 7714 (similar to the area of the dust emission) is given as only $1.7 \times 10^9 M_{\odot}$ compared to $7 \times 10^9 M_{\odot}$ for the whole system. Using this lower value would give a more reasonable value of 355 for $M_{\text{HI}}/M_{\text{d}}$, bringing G_{d} down to 802.

One further caveat to the whole $M_{\text{H}_2}/M_{\text{d}}$ business is the large discrepancies in the CO fluxes between single-dish measurements and interferometer mappings. Maps have been found for four of our galaxies (Sanders et al. 1988; Yun & Hibbard 1999; Laine et al. 1999) and always the flux is considerably less ($\leq 1/2$) than the single-dish measurement (Young et al. 1995). This is usually explained by resolution effects as these interferometer measurements are insensitive to structures larger than ~ 30 arcsec but even in sources unresolved by the interferometer at $cz \geq 10,000 \text{ km s}^{-1}$ (which are not expected to have large scale angular structure), the difference in flux is still as large. If we used the interferometer measurements for NGC 520, NGC 7469, NGC 7479 and UGC 4881, the corresponding H_2 masses would decrease by factors of 2, 2, 4, and 2 and bringing the $M_{\text{H}_2}/M_{\text{d}}$ ratios down to 229, 195, 163 and 260 respectively.

6 CONCLUSIONS

We have undertaken the first statistical survey of the local universe with the SCUBA bolometer array on the JCMT. We present here the initial results from the first of the samples we are surveying: a sample of 104 galaxies selected at $60\mu\text{m}$ from the *IRAS* Bright Galaxy Sample.

(i) The 60, 100 and $850\mu\text{m}$ fluxes are well fitted by single temperature SEDs. The mean and standard deviation (S.D.) in the best-fitting dust temperature is $\overline{T_{\text{d}}} = 35.6 \pm 4.9 \text{ K}$ with the mean and S.D. for the emissivity index being $\overline{\beta} = 1.3 \pm 0.2$. We do not however, rule out the possibility of colder dust and a steeper emissivity. If $\beta = 2$ and we assume there is a cold dust component with a temperature of 20 K, we then obtain dust masses a factor of 1.5–3 higher. The $450\mu\text{m}$ data obtained for 30 per cent of the galaxies may eventually constrain the submillimetre emissivity index and therefore the presence of a cold component.

(ii) We have presented the first direct measurements of the submillimetre luminosity and dust mass functions. They are well fitted by Schechter functions, in contrast to the *IRAS* $60\mu\text{m}$ LF (Lawrence et al. 1986; Rieke & Lebofsky 1986) which do not have the exponential cut-off required by the Schechter function. The slope of the $850\mu\text{m}$ LF at low luminosities is steeper than -2 implying that the LF must flatten at lower luminosities than were probed by this survey. The optically selected sample currently being observed will take the submillimetre LF to lower luminosities and constrain the ‘knee’ of the LF. The shape of the dust mass function is affected by the model assumed for the temperature distribution.

(iii) We have shown that a simple extrapolation of the *IRAS* $60\mu\text{m}$ LF to $850\mu\text{m}$ using a single dust temperature and emissivity index does not reproduce the measured submillimetre LF, both in terms of normalisation and shape.

(iv) A correlation was found between the fitted dust temperature and $60\mu\text{m}$ luminosity. This is best explained by the sensitivity of the $60\mu\text{m}$ flux to temperature (due to its position on the Wien side of the grey-body curve) rather than by a dependence on galaxy mass. Accounting for this temperature dependence when extrapolating the $60\mu\text{m}$ LF to submillimetre wavelengths produces a much better match to the observed $850\mu\text{m}$ LF.

(v) If there is a population of cold ($T_{\text{d}} < 25 \text{ K}$) galaxies which are also luminous submillimetre sources, then our submillimetre LF is likely to be biased, as these objects would not have appeared in the original *IRAS* bright galaxy sample which was selected at $60\mu\text{m}$. The question of a missing population will be addressed by the optically selected sample.

(vi) We find an average value for the gas-to-dust ratio (G_{d}) of 581 ± 43 where the gas mass is taken to be $M_{\text{HI}} + M_{\text{H}_2}$. This is lower than previous values determined using *IRAS* fluxes alone (~ 1000) indicating that the submillimetre is a better place to measure the dust mass. It is still, however, a factor of ~ 3.5 higher than the value obtained for the Galaxy (Sodroski et al. 1994). Using ‘cold dust masses’, calculated on the basis of there being a 20K component in addition to the warm dust, G_{d} was reduced to 293. This supports the idea that the previous large discrepancies in G_{d} for our own Galaxy (using *COBE* data), and

that of other galaxies (which use *IRAS* measurements), are due to a cold dust component which has gone undetected by *IRAS*.

(vii) The relationship between the mass of molecular hydrogen (as determined from CO observations) and dust mass shows very little intrinsic scatter (≤ 50 per cent) which implies that the CO to H₂ conversion, ‘X’, depends on metallicity in the same way as the dust mass.

(vii) The star formation efficiency as traced by $L_{\text{fIR}}/M_{\text{H}_2}$ was found to be anti-correlated with galaxy size (as measured by blue luminosity), a result also found by Young (1999) using a different technique. The star formation efficiency for these galaxies is higher on average than that for the Galaxy by a factor of ~ 3 (13.3 for the sample compared to 4 for the Milky Way).

FUTURE WORK

Observations which would further our understanding of the properties of dust in galaxies and refine our initial estimates of the LF are as follows:

- Shorter wavelength (300 – 600 μm) data from SCUBA and from SHARC on the CSO will allow us to ascertain the presence of any cold dust component in these galaxies and whether it is uniform (i.e. is the cold component similar in all the galaxies or does it vary as a function of some other property). Determining the existence of such a cold dust will allow a much more accurate estimate of the dust mass (and hence the dust mass function) to be made.
- In order to resolve some of the questions unanswered by this paper we will need to complete the survey of an optically selected sample. This will help to constrain the behaviour of the low luminosity end of the 850 μm LF (i.e. the turn-over) and also establish whether there is a population of ‘cold’ galaxies missing from this *IRAS* sample. We will then be able to investigate the differences between the *IRAS* galaxies when compared to ‘normal’ optically selected galaxies in terms of their dust properties.
- The 850 μm LF also requires more data points at the high luminosity end. This sample contained only a few very luminous objects because of the high flux limit for the BGS. Observations of a complete sample of ULIRGS at 850 μm would prove very useful in this respect.
- More CO and HI measurements, for those galaxies in both the *IRAS* and optically selected samples which do not have them already, would increase the statistical significance of the gas and dust comparisons. In addition, detailed mapping in both HI and CO would be of great importance in determining the relationship of the dust to the different gas phases of the ISM. Work on obtaining this data is in progress.
- Optical imaging would enable a comparison of the optical structures with those in the submillimetre. Of importance is the radial profile and scale height of the dust compared to the stars. Extinction maps could be created from multi-colour optical data and compared with the submillimetre maps, a technique described by Trewhealla (1998).

ACKNOWLEDGMENTS

We would like to thank all of the support staff at the JCMT as well as any observers who took data on our behalf when the conditions were too poor for their own projects. In particular, we are grateful to Wayne Holland for the ‘out of hours’ support after our runs were over. We also thank Paul Alton for useful discussions and information about NGC 891. The work of L. Dunne, S. Eales, M. Edmunds, R. Ivison and D. Clements is supported by PPARC.

REFERENCES

- Alton P. B. et al., 1998a, *A&A*, 335, 807
 Alton P. B., Bianchi S., Rand R. J., Xilouris E., Davies J. I., Trewhealla M., 1998b, *ApJ*, 507, L125
 Avni Y., Bahcall J. N., 1980, *ApJ*, 235, 694
 Barger A. J., Cowie L. L., Sanders D. B., Fulton E., Taniguchi Y., Sato Y., Kawara K., Okuda H., 1998, *Nat.*, 394, 248
 Barger A. J., Cowie L. L., Sanders D. B., 1999, *ApJ*, 518, L5
 Blain A. W., Kneib J.-P., Ivison R. J., Smail I., 1999a, *ApJ*, 512, L87
 Blain A. W., Smail I., Ivison R. J., Kneib J.-P., 1999b, *MNRAS*, 302, 632
 Bottinelli L., Gouguenheim L., Foque P., Paturel G., 1990, *A&AS*, 82, 391
 Cardelli J. A., Mathis J. S., Ebbets D. C., Savage B. D., 1993, *ApJ*, 402, L17
 Cardelli J. A., Meyer D. M., Jura M., Savage B. D., 1996, *ApJ*, 467, 334
 Casoli F., Dickey J., Kazès I., Boselli A., Gavazzi G., Jore K., 1996, *A&AS*, 116, 193
 Catalogued Galaxies and Quasars Observed in the *IRAS* Survey, 1989, Version 2. Prepared by Fullmer L., Lonsdale C. J. JPL, Pasadena
 Chini R., Krügel E., Lemke R., 1996, *A&AS*, 118, 47
 Clements D. L., Andreani P., Chase S. T., 1993, *MNRAS*, 261, 299
 Cox P., Krügel E., Mezger P. G., 1986, *A&A*, 155, 380
 Dalcanton J. J., Spergel D. N., Summers F. J., 1997, *ApJ*, 482, 659
 Davies J. I., Phillips S., Trewhealla M., Alton P. B., 1997, *MNRAS*, 291, 59
 Davies J. I., Alton P. B., Trewhealla M., Evans R., Bianchi S., 1999, *MNRAS*, 304, 495
 de Vaucouleurs G., de Vaucouleurs A., Corwin J. R., Buta R. J., Paturel G., Foque P., 1991, *The Third Reference Catalogue of Bright Galaxies*. Springer-Verlag, New York
 Devereux N. A., Young J. S., 1990, *ApJ*, 359, 42
 Draine B. T., Lee H. M., 1984, *ApJ*, 285, 89
 Dunlop J. S., Hughes D. H., Rawlings S., Eales S. A., Ward M. J., 1994, *Nature*, 370, 347
 Eales S. A., Edmunds M. G., 1996, *MNRAS*, 280, 1167 (EE96)
 Eales S. A., Edmunds M. G., 1997, *MNRAS*, 286, 732 (EE97)
 Eales S. A., Wynn-Williams C. G., Duncan W. D., 1989, *ApJ*, 339, 859
 Eales S. A., Lilly S. J., Gear W. K., Dunne L., Bond R. J., Hammer F., Le Fevre O., Crampton D., 1999, *ApJ*, 515, 518
 Edmunds M. G., Eales S. A., 1998, *MNRAS*, 299, L29
 Frayer D. T., Brown R. L., 1997, *ApJS*, 113, 221
 Frayer D. T., Ivison R. J., Smail I., Yun M. S., Armus L., 1999, *AJ*, 118, 139
 Garnett D. R., 1998, in Friedli D., Edmunds M. G., Robert C., Drissen L., eds, *ASP Conf. Ser. Vol. 147, Abundance Profiles: Diagnostic Tools for Galaxy History*. Astron. Soc. Pac., San Francisco, p. 78

- Genzel R. et al., 1998, *ApJ*, 498, 579
- Helou G., Soifer B. T., Rowan-Robinson M., 1985, *ApJ*, 298, L7
- Helou G., Khan I., Malek L., Boehmer L., 1988, *ApJS*, 68, 151
- Henry R. C. B., Worthey G., invited review to appear in *PASP* (astro-ph/9904017)
- Hildebrand R. H., 1983, *QJRAS*, 24, 267
- Holland W. S. et al., 1999, *MNRAS*, 303, 659
- Huchtmeier W. K., Richter O.-G., 1989, *A General Catalogue of HI Observations of Galaxies: The Reference Catalog*. Springer-Verlag, Berlin
- Hughes D. H., Robson E. I., Dunlop J. S., Gear W. K., 1993, *MNRAS*, 263, 607
- Hughes D. H., Dunlop J. S., Rawlings S., 1997, *MNRAS*, 289, 766
- Hughes D. H. et al., 1998, *Nat*, 394, 241
- Isaak K. G., McMahon R. G., Hills R. E., Withington S., 1994, *MNRAS*, 269, L28
- Issa M. R., MacLauren I., Wolfendale A. W., 1990, *A&A*, 236, 237
- Ivison R. J., 1995, *MNRAS*, 275, L33
- Jenness T., Lightfoot J. F., 1998, in Albrecht R., Hook R. N., Bushouse H. A., eds, *ASP Conf. Ser. Vol. 145, Astronomical Data Analysis Software & Systems VII*. Astron. Soc. Pac., San Francisco, p. 216
- Jenness T., Lightfoot J. F., Holland W. S., 1998, in Phillips T. G., ed, *Proc. SPIE. Vol. 3357, Advanced Technology MMW, Radio & Terahertz Telescopes*, p. 548
- Kenney J. D. P., Young J. S., 1989, *ApJ*, 344, 171
- Laine S., Kenney J. D. P., Yun M. S., Gottesman S. T., 1999, *ApJ*, 511, 709
- Lavezzi T. E., Dickey J. M., 1998, *AJ*, 115, 405
- Lawrence A., Walker D., Rowan-Robinson M., Leech K. J., Penston M. V., 1986, *MNRAS*, 219, 687
- Lawrence A. et al., 1999, *MNRAS*, 308, 897
- Lilly S. J., Le Fevre O., Hammer F., Crampton D., 1996, *ApJ*, 460, L1
- Lilly S. J., Eales S. A., Gear W. K., Hammer F., Le Fevre O., Crampton D., Bond R. J., Dunne L., 1999, *ApJ* accepted, astro-ph/9901047
- Madau P., Ferguson H. C., Dickinson M. E., Giavalisco M., Steidel C. C., Fruchter A., 1996, *MNRAS*, 238, 1388
- Maiolino R., Ruiz M., Rieke G. H., Papadopoulos P., 1997, *ApJ*, 485, 552
- Maloney P., 1990, in Thronson H. A. Jr., Shull J. M., eds, *The Interstellar Medium in Galaxies*. Kluwer, Dordrecht, p. 493
- Masi S. et al., 1995, *ApJ*, 452, 253
- Meyer D. M., Jura M., Cardelli J. A., 1996, *ApJ*, 493, 222
- Papadopoulos P. P., Seaquist E. R., 1999, *ApJ*, 514, L95
- Press W. H., Schechter P., 1974, *ApJ*, 187, 425
- Reach W. T. et al., 1995, *ApJ*, 451, 188
- Rieke G. H., Lebofsky M. J., 1986, *ApJ*, 304, 326
- Rigopoulou D., Lawrence A., Rowan-Robinson M., 1996, *MNRAS*, 278, 1049
- Sanders D. B., Mirabel I. F., 1985, *ApJ*, 298, L31
- Sanders D. B., Young J. S., Soifer B. T., Schloerb F. P., Rice W. L., 1986, *ApJ*, 305, L45
- Sanders D. B., Soifer B. T., Scoville N. Z., Sargent A. I., 1988, *ApJ*, 324, L55
- Sanders D. B., Scoville N. Z., Soifer B. T., 1991, *ApJ*, 370, 158
- Schechter P., 1975, PhD thesis, California Institute of Technology
- Scoville N. Z., Good J. C., 1989, 339, 149
- Smail I., Ivison R. J., Blain A. W., 1997, *ApJ*, 490, L5
- Smail I., Ivison R. J., Blain A. W., Kneib J.-P., 1998, *ApJ*, 507, L21
- Smith B. J., Struck C., Pogge R. W., 1997, *ApJ*, 483, 754
- Sodroski T. J., Dwek E., Hauser M. G., Kerr F. J., 1989, *ApJ*, 336, 762
- Sodroski T. J. et al., 1994, *ApJ*, 428, 638
- Soifer B. T., Sanders D. B., Madore B. F., Neugebauer G., Danielson G. E., Elias J. H., Lonsdale C. J., Rice W. L., 1987, *ApJ*, 320, 238
- Soifer B. T., Boehmer L., Neugebauer G., Sanders D. B., 1989, *AJ*, 98, 766
- Solomon P. M., Downes D., Radford S. J. E., Barrett J. W., 1997, *ApJ*, 478, 144
- Stark A. A., Davidson J. A., Platt S., Harper D. A., Pernic R., Loewenstein R., Engargiola G., Casey S., 1989, *ApJ*, 337, 347
- Surace J. A., Mazzarella J., Soifer B. T., Wehrle A., 1993, *AJ*, 105, 864
- Theureau G., Bottinelli L., Coudreau-Durand N., Gouguenheim L., Hallet N., Loulergue M., Paturel G., Teerikorpi P., 1998, *A&AS*, 130, 333
- Trewhella M., 1998, *MNRAS*, 297, 807
- Whittet D. C. B., 1992, *Dust in the Galactic Environment*. Institute of Physics, Bristol
- Wilson C. D., 1995, *ApJ*, 448, L97
- Young J. S., Xie S., Kenney J. D. P., Rice W. L., 1989, *ApJS*, 70, 699
- Young J. S. et al., 1995, *ApJS*, 98, 219
- Young J. S., 1999, *ApJ*, 514, L87
- Yun M. S., Hibbard J. E., 1999, submitted to *ApJ*, astro-ph/9903463